

Masters Program in **Geospatial Technologies**



***Solving the latency problem in Real-time GNSS Precise
Point Positioning using open source software***

Mutaz Wajeh Abdlmajid Qafisheh

Dissertation submitted in partial fulfilment of the requirements
for the Degree of *Master of Science in Geospatial Technologies*

**Solving the latency problem in Real-time GNSS Precise Point
Positioning using open source software**

Dissertation supervised by

Joaquín Huerta, PhD

Professor at Institute New Imaging Technologies,

University Jaume I,

Castellón, Spain

Dissertation co-supervised by

Ángel Martín, PhD

Professor at Department of Engineering Cartographic Geodesy and photogrammetry,

Universitat Politècnica de València UPV,

València, Spain

Dissertation co-supervised by

Marco Painho, PhD

Professor at NOVA Information Management School,

Universidade Nova de Lisboa,

Lisbon, Portugal

March 2020

Acknowledgments

First of all, I would like to thank Allah for all the gifts and blessings and for giving me the ability and the courage to proceed and conduct this thesis. I want to express my deep thanks to all the professors who taught me in this study, especially for my master thesis supervisor's professor Joaquín Huerta and professor Marco Painho. I would like to express special thanks to Professor Sven Casteleyn, who motivated me to continue programming and solving errors and keep fight till the success. I would like to thanks Elena Martínez for her administrative guidance and support.

I am grateful to the Erasmus Mundus program for providing the scholarship to pursue my Masters in Geospatial Technologies. I received a great opportunity to improve my educational, communication skills, and cultural awareness. Deep thanks in particular to my colleagues, who I now consider as a big family.

I would like to acknowledge the Universitat Politècnica de València for offering all the infrastructure required to accomplish this study. Deep thanks to my supervisor Angel Martin from Universitat Politècnica de València for a long trip of guidance, supervision, and for the acceptance to persuade the Ph.D. studies in Universitat Politècnica de València.

Last but not least, I would also like to thank my family, who supported me and have enough faith in me, especially my father, wife, and daughters—warm regards to my youngest sister for proofreading this thesis.

Solving the latency problem in Real-time GNSS Precise Point Positioning using open source software

ABSTRACT

Real-time Precise Point Positioning (PPP) can provide the Global Navigation Satellites Systems (GNSS) users with the ability to determine their position accurately using only one GNSS receiver.

The PPP solution does not rely on a base receiver or local GNSS network. However, for establishing a real-time PPP solution, the GNSS users are required to receive the Real-Time Service (RTS) message over the Network Transported of RTCM via Internet Protocol (NTRIP). The RTS message includes orbital, code biases, and clock corrections.

The GNSS users receive those corrections produced by the analysis center with some latency, which degraded the quality of coordinates obtained through PPP. In this research, we investigate the Support Vector Machine (SVR) and RandomForest (RF) as machine learning tools to overcome the latency for clock corrections in the CLK11 and IGS03 products. A BREST International GNSS Services permanent station in France selected as a case study. BNC software implemented in real-time PPP for around three days. Our results showed that the RF method could solve the latency problem for both IGS03 and CLK11. While SVR performed better on the IGS03 than CLK11; thus, it did not solve the latency on CLK11. This research contributes to establishing a simulation of real-time GNSS user who can store and predict clock corrections accordingly to their current observed latency.

The self-assessment of the reproducibility level of this study has a rank one out of the range scale from zero to three according to the criteria and classifications are done by (Nüst et al., 2018).

KEYWORDS

Real-time Precise Point Positioning

Global Navigation Satellite systems

Latency

International GNSS Services products

Support Vector Regression

RandomForest

Clock corrections predictions

ACRONYMS

- APC** - Antenna Phase Center
- CART** - Classification and Regression Tree
- CV** - Cross-Validation
- DLR** - German Aerospace Center
- ECEF** - Earth Center Earth Fixed
- GBM** - Geodetic Benchmark
- GNSS** - Global Navigation Satellite System
- ITRF** - International Terrestrial Reference Frame
- MC** - Mass Center
- MSC** - Master Control Station
- NTRIP** - Network Transported of RTCM via Internet Protocol
- PPP** - Precise Point Positioning
- RBF** - Radial Base Function
- RETICLE** - Real-Time Clock Estimation
- RF** - RandomForest
- RINEX** - Receiver Independent Exchange Format
- RMS** - Root Mean Squared
- RSS** - Residual Sum of Squares
- RTC** - Real-Time Correction
- RTK** - Real-Time Kinematic
- RTS** - Real-Time Services
- SP3** - Standard Product #3
- SSR** - State-Space Representation
- SVC** - Support Vector Classifier

SVM - Support Vector Machine

SVR - Support Vector Regression

TEC - Total Electron Content

TVEC - Total Vertical Electron Content

UHF - Ultra-Higher Frequency

VRS - Virtual Reference Station

WP - Work Packages

INDEX OF THE TEXT

Acknowledgments	III
ABSTRACT.....	IV
KEYWORDS.....	V
ACRONYMS.....	VI
INDEX OF THE TEXT	VIII
INDEX OF TABLES	X
INDEX OF FIGURES	XI
Chapter 1 Introduction	1
1.1 Motivation.....	1
1.2 Research Question	3
1.3 Thesis Organization	5
Chapter 2 Background	6
2.1 Literature review	6
2.2 GNSS Measurement background.....	8
2.3 Cycle slip	11
2.4 Ambiguity resolution	12
2.5 GNSS errors	12
2.6 Precise Point Positioning	21
2.7 Machine learning	23
2.8 BNC Software overview	28
2.9 Python and complementary libraries	29
Chapter 3 Research Methodology.....	30
3.1 WP1 General reviewing.....	30
3.2 WP2 IGS products and stations	30
3.3 WP3 Data preparation.....	32
3.4 WP4 Machine learning	34
3.5 WP5 Visualization	36
3.6 WP6 Statistical assessment.....	36
Chapter 4 Results and discussions	38
4.1 Latency values	38
4.2 Support vector regression parameter	38
4.3 Support vector regression R2 score and different kernel.....	41
4.4 Support vector regression and RandomForest in real-time simulation.....	42
Chapter 5 Conclusion and Future works.....	59

5.1 Conclusion	59
5.2 Future works	61
References.....	62

INDEX OF TABLES

Table 2-1 IGS Clock products (The International GNSS Service, 2013)	13
Table 2-2 IGS Orbit products (The International GNSS Service, 2013)	14
Table 3-1 Brest coordinates (IGS, 2020)	31
Table 3-2 sample of the data in the created CLK data frame.....	33
Table 3-3 the final CLK data frame with latency values	34
Table 4-1 IGS03 and CLK11 statistical summary of latency values	38
Table 4-2 C and gamma values.....	39
Table 4-3 results of C and gamma for the IGS03 corrections.....	40
Table 4-4 results of C and gamma for the CLK11 corrections	41
Table 4-5 R ² score values for different kernels IGS03	42
Table 4-6 R ² score values for different kernels CLK11	42
Table 4-7 IGS03 SVR statistical assessment for GPS satellites	45
Table 4-8 IGS03 SVR statistical assessment for GLONASS satellites	46
Table 4-9 IGS03 SVR statistical assessment for GPS satellites	47
Table 4-10 IGS03 SVR statistical assessment for GLONASS satellites	48
Table 4-11 CLK11 SVR statistical assessment for GPS satellites.....	49
Table 4-12 CLK11 SVR statistical assessment for GLONASS satellites.....	50
Table 4-13 IGS03 RF statistical assessment for GPS satellites	53
Table 4-14 IGS03 RF statistical assessment for GLONASS satellites	54
Table 4-15 CLK11 RF statistical assessment for GPS satellites.....	56
Table 4-16 CLK11 RF statistical assessment for GLONASS satellites.....	57
Table 5-1 IGS03 SVR statistical assessment summary	59
Table 5-2 IGS03 SVR statistical assessment summary	60
Table 5-3 CLK11 SVR statistical assessment summary.....	60
Table 5-4 IGS03 RF statistical assessment summary	60
Table 5-5 CLK11 RF statistical assessment summary.....	60

INDEX OF FIGURES

Figure 1-1 Vale coordinates residual for CLK11 with 10-15 seconds latency	4
Figure 1-2 Vale coordinates residual for IGS03 with 35-40 seconds latency	4
Figure 2-1 Range measurement timing relationships.....	9
Figure 2-2 Positioning determination in 3-dimensional space.....	10
Figure 2-3 Phase measurements illustration	11
Figure 2-4 Along-track, cross-track and radial orbital components.....	14
Figure 2-5 IGS conventional Antenna Phase Center in Satellite Fixed reference frame	15
Figure 2-6 Receiver and monument centers	16
Figure 2-7 Multipath Error	17
Figure 2-8 Ionosphere and troposphere layer.....	18
Figure 2-9 Overview of GNSS errors	21
Figure 2-10 The solid black line defined the hyperplane separated the two classes of data	24
Figure 2-11 The support vectors use for maximal margin hyperplane	25
Figure 2-12 SVM margin.....	27
Figure 2-13 Effect of using different values of gamma	27
Figure 2-14 BNC Software interface	29
Figure 3-1 Brest station receiver mount point	31
Figure 3-2 Brest station location.....	32
Figure 3-3 CLK11 text file CLK11.....	33
Figure 3-4 CLK coordinates and latency value text file	34
Figure 3-5 Potentiality of SVR in solving latency	35
Figure 3-6 Real-time simulation	36
Figure 3-7 Statistical assessment of simulation phase	37
Figure 4-1 SVR with default parameters	39
Figure 4-2 SVR with predefined parameters	40
Figure 4-3 IGS03 30 seconds of latency effect on the satellite G01	43
Figure 4-4 CLK11 10 seconds of latency effect on the satellite G01	44
Figure 4-5 IGS03 SVR model for satellite G01.....	51
Figure 4-6 IGS03 histogram of the differences obtained by the SVR method for satellite G01.....	51
Figure 4-7 CLK11 SVR model for satellite G01	52
Figure 4-8 CLK11 histogram of the differences obtained by the SVR method for satellite	52
Figure 4-9 IGS03 RF model for satellite G01.....	55
Figure 4-10 IGS03 histogram of the differences obtained by the RF method for satellite G01.....	55
Figure 4-11 CLK11 RF model for satellite G01	58
Figure 4-12 CLK11 histogram of the differences obtained by the RF method for satellite G01	58

Chapter 1 Introduction

1.1 Motivation

The number of operational navigation satellites has been increased by the last decade. In December 2019, the GNSS consisted of 108 operational satellites. Further information about current constellations status can be found in (European GNSS Service Centre, 2020; Information and Analysis Center, 2020).

The navigation users rely on those operational satellites to calculate their position. However, PPP is one of many position techniques, has been used for positioning determination. It is driven by cost reduction as a consequence of using one receiver and the availability of using this method in a global scope. This resulted in widespread using PPP in many areas and applications. Many studies sought potential areas where this method can be used. (Barker, Lapucha, & Wood, 2002) discussed the potential areas where the usage of PPP will take place, like offshore and sea construction; these areas suffer from lack of coverage of nearby base GNSS stations, or they are not covered by GNSS network solution or Virtual Reference Station (VRS). These isolated areas or regions with fewer infrastructures can take advantage of this technique. (Bezioglu, Yigit, & El-mowafy, 2019) examined the PPP methods in the Antarctic regions. On the contrary, traditional GNSS methods have limitations to use in those regions due to the fact of the high initialization cost and maintenance difficulties because of the harsh weather conditions.

Increasing world population results in a huge urban expansion; therefore, the demand for building megastructures like dams, bridges, and skyscrapers is also increasing. Monitoring such structures is crucial to protect lives and prevent economic losses. Structural monitoring using real-time PPP has been sought by many researchers (Beskhyroun, Wegner, & Sparling, 2011; Hristopulos, Mertikas, Arhontakis, & Brownjohn, 2007; Kaloop, Elbeltagi, Hu, & Elrefai, 2017; Khoo, Tor, & Ong, 2010; Rizos & Cranenbroeck, 2010). Real-time PPP for bridge monitoring done by (Tang, Roberts, Li, & Hancock, 2017).

Climate change and the greenhouse effect bring high rainfall storms; therefore, the frequency of occurring the landslides incidents event increased as well; real-time PPP

for landslide monitoring investigated by (Capilla, Berné, Martín, & Rodrigo, 2016; Cina & Piras, 2015; Şanlıoğlu, Zeybek, & Özer Yiğit, 2016).

Different studies investigated real-time PPP in the domain of deformation monitoring (Martín, Anquela, Dimas-Pagés, & Cos-Gayón, 2015; Piras & Roggero, 2009; Shi, Xu, & Guo, 2013; Zhiping Liu, 2016). The requirements, challenges, and benefits of establishing the early warning system for Tsunami and earthquake researched in (Blewitt et al., 2009; Labrecque, Rundle, & Bawden, 2018; Wächter et al., 2012). A simulation study done by (Capilla et al., 2016) showed the possibility of using real-time PPP for establishing an early warning system. Real-time PPP for natural hazard warning system sought by (El-Mowafy, 2019; El-Mowafy & Deo, 2017).

Clocks, orbits, and other real-time corrections are essential to perform real-time PPP. The IGS began the real-time Pilot project in 2007. The following analysis centers participate in this pilot project: BKG, CNES, DLR, ESA/ESOC, GFZ, GMV, NRCan, and Wuhan University. The project aims to maintain and track real-time GNSS network stations, as well as compute and broadcast clock and orbit corrections for real-time users. Since 2013 IGS RTS have been disseminated for real-time users. Additionally, the multi GNSS Experiment and pilot project (MGEX) disseminate the Real-Time Correction (RTC) for all GNSS signals (The Multi-GNSS Experiment and Pilot Project (MGEX), 2016). IGS and MGEX freely disseminate the RTC products through NTRIP (Weber, Dettmering, & Gebhard, 2005). Other company solutions such as VERIPOS, TerraStar, OmniSTAR, RTX, and StarFire can be found in (Fugro, 2016; NovAtel, 2015; Trimble, 2012). Real-time corrections disseminate from analysis centers suffer by some latency values, the values of latency vary, and it increases remarkably for combined products.

Currently, the IGS and other analysis centers still provide real-time corrections which are received by the GNSS users with latency vary between 5-10 seconds for individual products; however, it could reach around 30 seconds for the combined products.

The novel contribution to this research is to use the support vector regression and RandomForest as a machine learning tool to overcome the latency problem in CLK11 and IGS03 products. The methodology applied to this research is also applicable to other IGS products.

1.2 Research Question

The International GNSS services, as well as the analysis centers disseminating Real-time service to implement corrections for GNSS observations. However, those corrections arrived at real-time GNSS users with some seconds of latency. The latency can define as a delay in receiving the corrections from the analysis centers, and this time delay could be around a couple of tens seconds.

The research question in this thesis research is, *“How can the Machine learning solve the latency problem in real-time products?”*

The linear model joint with the periodic term is a classic model used for predicting the clock corrections. The improvement of this model to adapt different GPS clock satellites done by (G. W. Huang, Zhang, & Xu, 2014). (Martín, Hadas, Dimas, & Anquela, 2013) concluded that the quality of coordinates obtained by real-time PPP is highly correlated with latency values. Figures 1.1 and Figure 2.1 show the differences between the true coordinates of the Vale station with respect to the observed coordinates -those differences called a coordinate residual-, the residual of Vale station in Valencia are shown in terms of: North, East ,and up (height). Figures 1.1 and Figure 2.1 show the effect of 10-15 and 35-45 seconds of latency respectively.

In order to find an answer to this research question, the support vector regression, and RandomForest as a machine learning tool could be extended to extrapolate the clock corrections without concerning about the type of the navigation satellite system. Solving latency problems in real-time services will improve the accuracy of the position obtained by real-time PPP users. Consequently, it will open the doors for the PPP method for more involvement in different applications and areas.

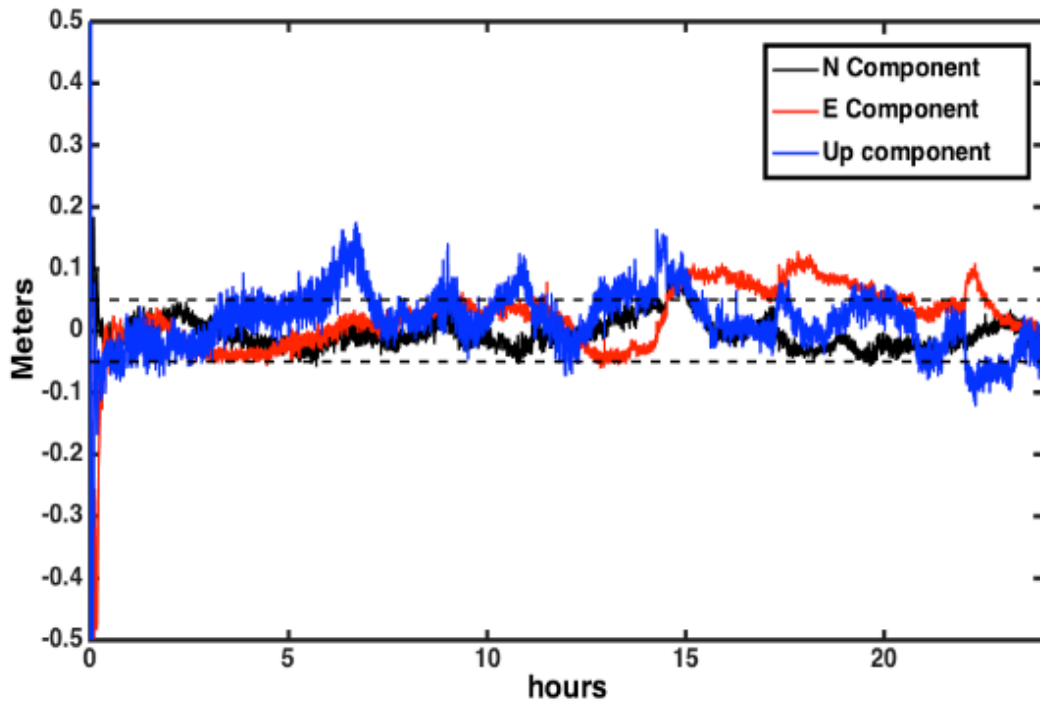


Figure 1-1 Vale coordinates residual for CLK11 with 10-15 seconds latency (Martín et al., 2013)

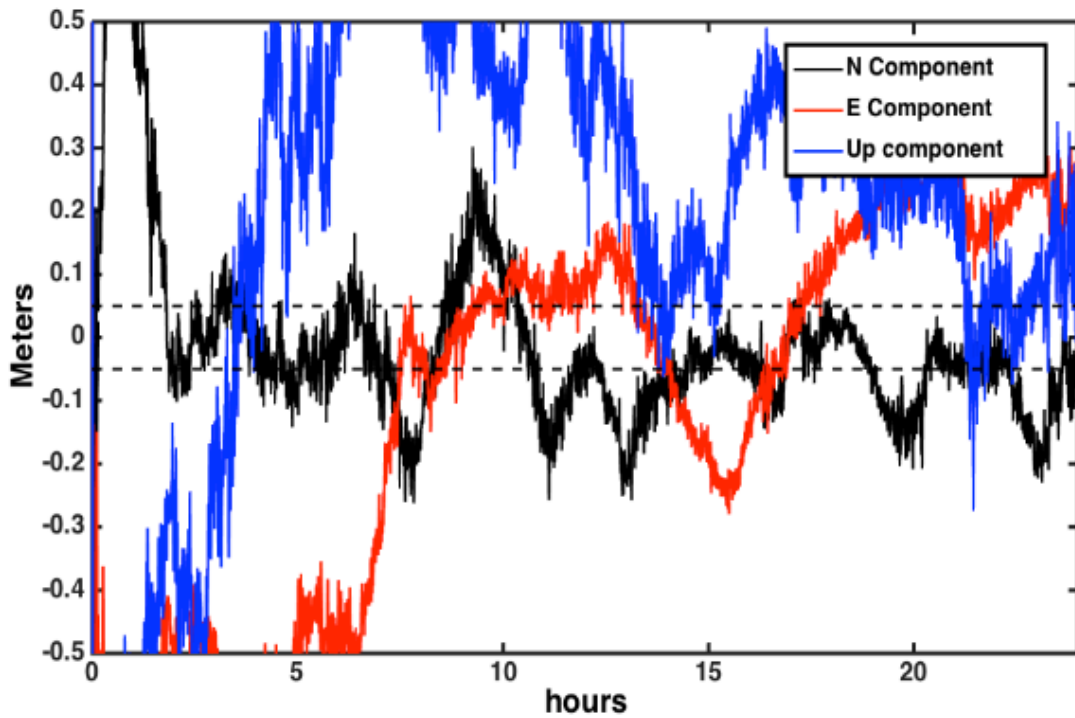


Figure 1-2 Vale coordinates residual for IGS03 with 35-40 seconds latency (Martín et al., 2013)

1.3 Thesis Organization

This is a complete overview of the thesis dissertation organization. The dissertation is composed of five chapters.

Chapter 2 is a background chapter. It starts with state-of-the-art, including relevant research on the field, followed by definitions of terms and concepts that are used throughout the dissertations.

Chapter 3 is the methodology chapter that contains explanations of the different steps performed in this research. The explanations will be abstracted and explained in text and flow charts.

Chapter 4 is the results chapter that contains explanations, discussions, and statistical assessments of the results obtained in this research. This chapter includes an illustration of the results with numerical tables and graphical figures.

Chapter 5 is the concluding chapter that contains summarized tables and a comparison between the methods used in this research, and it ends with recommendations, suggestions, and for future works.

Chapter 2 Background

This chapter aims to provide a general idea of the topics included in this research, a brief description of the mathematical equations has been developed in GNSS, a summary of pseudorange methods, as well as descriptions to different sources of errors in GNSS system. Moreover, an overview of the PPP method and BNC software can found in the middle of this chapter. This chapter ends with an explanation of the machine learning tools used in this research.

2.1 Literature review

The GNSS is widely used for positioning determination. Different techniques, such as stand-alone positioning, PPP, and differential GNSS, which includes real-time kinematic, static, and virtual reference stations, have been implemented for positioning determination (Blewitt, 2019). Consequently, the quality of the determined position, observation period, and the quality of used GNSS receivers are varied among different techniques.

The advent of the PPP method allows the GNSS users to reach sub decimetre accuracy using only a single GNSS receiver, taking into account this method can use on a global scale. The PPP method was firstly introduced by (Zumberge, Heflin, Jefferson, Watkins, & Webb, 1997). GNSS users can implement the PPP method in real-time and post-process. In order to reach such accuracy in real-time; the PPP method requires precise orbit corrections, codes and phases biases, and clock corrections. The International GNSS Services and different analysis centers are responsible for the generation and broadcasting of high accurate GNSS data and products. Those products include orbits and clock corrections, earth orientation, Tropospheric, and Ionospheric parameters besides the code and phase biases (Johnston, Riddell, & Hausler, 2017). The IGS products serve both real-time and post-process GNSS users. In 2013 the International GNSS Services launched real-time services to provide GNSS users with real-time corrections (The International GNSS Service, 2013).

The performance of real-time PPP was sought by (Chen et al., 2013). In this research, the analysis of the collected data during one month concluded that real-time clock corrections products could meet the correctness of IGS ultra rapid (IGU).

The satellite clock corrections are suffering from a high variation; according to the changing of satellite locations and temperature variation. (Yao, He, et al., 2017) studied the evaluation and comparison of the satellite clock offsets using the estimation of real-time clock offset with a linear model after resolving the initial clock bias. The stability of IGS clock products in terms of daily bases variation sought by (Senior, Ray, & Beard, 2008).

A precision of 20 cm and 15 minutes converging time was achieved by (L. Wang et al., 2018). In this study, the CLK93 was used for orbital and clock corrections. The IGS03 products were used for performing real-time PPP. A precision of sub-decimeter with 20 minutes conversion time obtained by (Alcay & Turgut, 2017). (Shi et al., 2013) concluded that the centimeter to a sub-decimeter level of precision with 10 minutes conversion time can be achieved using CLK90 product. Additionally, (Shi et al., 2013) made a comparison between CLK93 with final IGS products determined that 4.57 cm and 0.5 ns a three-dimensional orbit and clock accuracy repetitively can be achieved in real-time.

Different real-time products are assessed by (Z. Wang, Li, Wang, Wang, & Yuan, 2018). In this recent study, the assessment done by linking the difference between different real-time products and Geodetic Benchmark (GBM).

The effect of Ionospheric impact on real-time PPP was investigated by (Erdogan & Karlitepe, 2016). In this study, CLK91 was used for establishing real-time PPP; the result found the considerable difference of obtained coordinates for one IGS station located in the tropical region occurred in the mid-day period affected by strong ionospheric influence. The Enhancement of real-time PPP and post-process PPP by implemented different techniques sought by (Juan et al., 2012; Yao, Peng, Xu, & Cheng, 2017).

The sinusoid as aperiodic function joint with the linear model has been chosen as a model for many researchers, and different clock types are deployed in GPS satellites, Consequently (G. W. Huang et al., 2014) improved the conventional model to adapt the variation resulting from using different types of clocks. The same clock model used to predict the clock corrections for a long timestamp by (El-Mowafy, 2019; El-Mowafy, Deo, & Kubo, 2017). The two studies proved the efficiency of using the conventional clock model to accommodate periods of absence of internet

communication. Kalman filter is another method for predicting clock corrections studied in the research done by (G. Huang & Zhang, 2012). The dataset obtained from 129 stations during 2015 used to model the daily variation of the inter-frequency clock bias, with one centimeter level of prediction accuracy (Yuan et al., 2018). The effect of the different intervals of updating the clock offset investigated (Yang, Xu, & Gao, 2019). The evaluation of real-time products in terms of latency and availability examined by (Hadas & Bosy, 2014).

Additionally, Hadas remarked that latency affects remarkably the combined IGS products. Hadas made a comparison which conducted between REal-Time Clock Estimation (RETICLE) with IGS combined product. The German Aerospace Centre is responsible for the dissemination of the RETICLE service used for clock and orbit corrections. The latency effect IGS combined product more than products obtained individually by different analysis centers; subsequently, the combined product did not lead to better outcomes rather than RETICLE (Martín et al., 2015).

The investigation research on latency for real-time PPP done by using both of the CLK11 and the IGS03; accordingly, the latency with 10 and 40 seconds is introduced repressively to both products. The accuracy of the obtained results showed a high correlation with latency (A.Martin, T Hadas, Dimas, & Anquela, 2013). Different computational methods examined by (Ge, Chen, Douša, Gendt, & Wickert, 2012) to reduced real-time clock corrections computational time. The current research investigates the ability to predict clock corrections using machine learning tools.

2.2 GNSS Measurement background

GNSS is a timing measuring system, in other words, the GNSS users need to know the transmitted and received time of the GNSS signals, different types of clocks are deployed on GNSS satellites and GNSS receivers. Knowing the signal travel time and the speed of the travel signal, consequently, the distance between the satellite and user can be calculated, and it symbolized as pseudorange. Knowing the exact locations and distances of GNSS satellites, thus the GNSS users can determine their locations.

The GNSS satellites transmit their signals in the L band. The L band is a part of the Ultra-Higher Frequency (UHF) spectrum. GPS L1, GLONASS G1 and Galileo E1 signals are located in the band 1559-1610 MHz, GPS L2, GLONASS G2, and Galileo

E2 signals are located in the band 1215-1350 MHz, where GPS L5, GLONASS G5, and Galileo E5 signals are located in the band 1164-1215 MHz (Enge & Misra, 2011).

2.2.1 Code Pseudorange

The elementary measurement of the GNSS receiver is the measuring of the time difference between transmitted and received time of the arrival signals. This is done by aligning the code generated locally inside the receiver with the arrived signals via the correlation method (Enge & Misra, 2011). The precision of the calculated pseudorange is around 1% of the chip length (Wells, 1999). For example, in the GPS, according to the type of code, the pseudorange precision varies between 0.3 to 3 meters (B.Hoffmann-Wellenhof & H.Lichtenegg, 2001). The pseudorange measurement suffering mainly with clock biases due to the reality both of the satellite and receiver clock are not synchronized concerning the common time system (Enge & Misra, 2011). The following equations and figure show the pseudorange calculations.

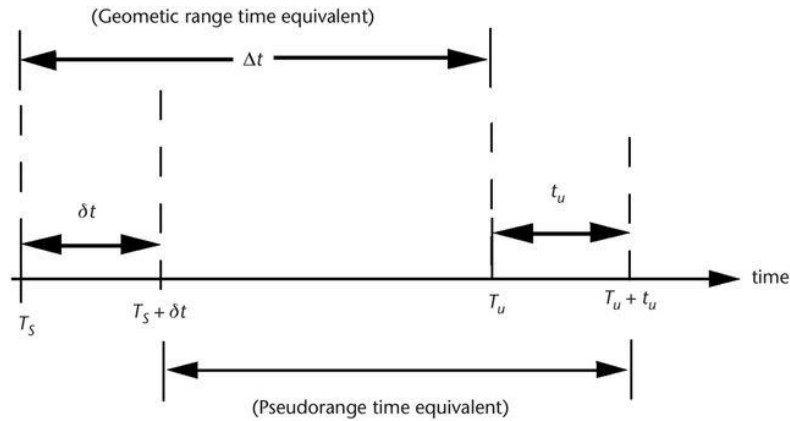


Figure 2-1 Range measurement timing relationships(Kaplan & Hegrat, 2006)

$$\Delta t = T_U - T_S = [T_U + t_U] - [T_S + \delta t] \quad 2.1$$

Where T_S and T_U denote respectively the transmitted and received time for the GNSS signal, δt is the satellite clock bias with respect to common reference time GNSS system, t_U is the receiver clock bias.

$$\rho = c[T_U + t_U] - [T_S + \delta t].$$

$$\rho = c(T_U - T_S) + c(t_U - \delta t).$$

$$r = c(T_U - T_S) = c * \Delta t.$$

$$\rho = r + c(t_U - \delta t) \quad 2.2$$

Where ρ denote the pseudorange, r is the geometric distance between the satellite and the GNSS user, while the speed of light denoted as c .

The last pseudorange equation can be modified by introducing the error influence by the troposphere and Ionosphere, and other types of errors (Kaplan & Hegrat, 2006), more information about GNSS errors can be found in the [error section](#) in this chapter.

$$\rho = r + c(t_U - \delta t) + I_\rho + T_\rho + \xi_\rho \quad 2.3$$

Where I_ρ and T_ρ denote respectively the propagation of the GNSS signals through the ionospheric and tropospheric layer, and ξ_ρ denote other sources of error.

The minimum number of GNSS satellites required for positioning determination is four satellites to solve the position in three-dimensional space (Polland, 2009). Figure 2.2 shows four GNSS satellites uses for positioning determination.

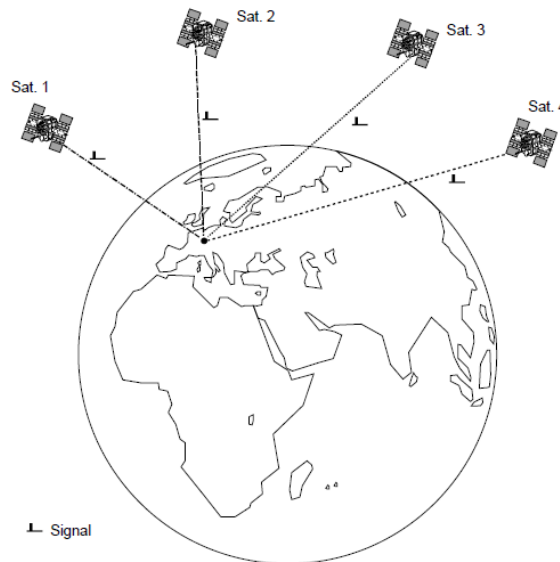


Figure 2-2 Positioning determination in 3-dimensional space(Polland, 2009)

2.2.2 Phase Pseudorange

Reaching a precision of 0.3 to 3 meters in pseudorange is not acceptable in some applications (NovAtel Inc, 2015). Sub centimeter precision is achievable by implementing the carrier phase measurement (Wells, 1999). By counting the total number of the full carrier phase with a fractional cycle between satellite and user. Consequently, the range can obtain by multiplication that number with a wavelength of the carrier (Polland, 2009). The following figure illustrates the principle of phase measurement.

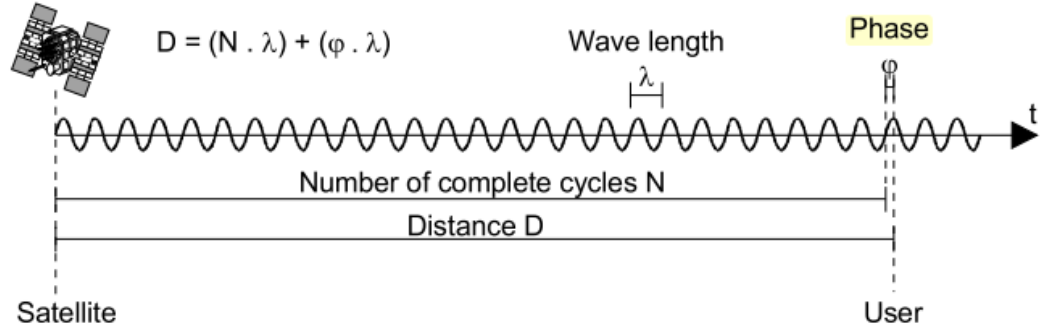


Figure 2-3 Phase measurements illustration (Polland, 2009)

$$D = (N * \lambda) + (\phi * \lambda) \quad 2.4$$

Where D is the pseudorange between the satellite and GNSS users, N is the number of the complete cycles between the satellite and user, λ denote the wavelength of the arrival signal, and ϕ is the fraction of the cycle measured by the GNSS receiver.

The main two weaknesses of this method that firstly, the receiver cannot know the exact number N of the complete cycle between the satellite and user. This is the reason behind calling it the ambiguity number. Secondly, the receiver needs to keep count and track the arrival phase, which some time suffers from cycle slips (Wells, 1999). PPP and Real-Time Kinematic (RTK) use a different technique for solving the ambiguity number for reaching the level of centimeter accuracy (NovAtel Inc, 2015). The influence of tropospheric and Ionospheric layers affects the pseudoranging equation. Thus the last equation can be modified as:

$$\phi = \lambda^{-1} [r + I_{\phi} + T_{\phi}] + \frac{c}{\lambda} (\delta_{tu} - \delta_{ts}) + N + \xi_{\phi} \quad 2.5$$

Where ϕ represent the number of carrier cycle between GNSS satellite and GNSS user, λ is the carrier wavelength, while I_{ϕ}, T_{ϕ} denote respectively the ionosphere and troposphere propagation delay in meter, N is the integer number of carrier cycles, δ_{tu}, δ_{ts} denote respectively the GNSS receiver and satellite clock biases, C is the speed of light, and ξ_{ϕ} denote other sources of noise.

2.3 Cycle slip

As mentioned before, one of the weaknesses of phase carrier measurement is the occurrence of the cycle slip. Through the tracking period, the GNSS receiver needs to keep counting the fractional of the carrier cycle. On every occasion, the fractional

phase fluctuates from 360 to 0 degrees, one cycle will add to the initial cycle counts (B.Hoffmann-Wellenhof & H.Lichtenegg, 2001). The cycle slip can define as "a jump of the number of integer cycles" (NovAtel Inc, 2015). These jumps may occur according to the surrounding environmental conditions such as tree leaves, buildings, and power lines. Receiver hardware manufacturing quality besides the software capabilities could also lead to the occurrence of cycle slip (B.Hoffmann-Wellenhof & H.Lichtenegg, 2001).

2.4 Ambiguity resolution

The elementary four unknowns in GNSS measurements are the user position (X, Y, Z) in three-dimensional space plus the receiver clock bias. New unknown in equation 2.5, N which indicate the integer number of cycles between the GNSS user and satellite (NovAtel Inc, 2015) called ambiguity, different approaches for solving the ambiguity are implemented such as single frequency, dual-frequency, dual-frequency combining code and phase measurements and triple frequency (B.Hoffmann-Wellenhof & H.Lichtenegg, 2001). All the pre mention approaches are depending on running two GNSS receivers simultaneously. The length between both receivers called the baseline; the precision of a determined position is highly dependent on baseline length, and it is recommended not to exceed 20 Km (Enge & Misra, 2011). Development in solving the ambiguity number can be found in (Geng, 2016; Juan et al., 2012).

2.5 GNSS errors

The GNSS measurements suffer from three types of error. Firstly blunders or outliers and those measurements must be removed from the sample of measurements. Secondly, systematic errors that follow the environmental or physical law; thus, this type of error can be removed by applying measurement modeling. Finally, the random error, which is small quantities of errors remains after eliminating blunders and systematic errors (Wolf & Wiley, 2006). During military activates, errors are intentionally introduced to the system (NovAtel Inc, 2015). This error called in GPS selective availability (El-Rabbany, 2002). Code and phase measurements together are affected by these errors (B.Hoffmann-Wellenhof & H.Lichtenegg, 2001).

2.5.1 Satellite clock errors

Atomic clocks, mainly Rubidium or Cesium, are deployed on-boarded GNSS satellites. Frequency drift and frequency offset affected the clock oscillator (Wells, 1999). An error of 10 Nanoseconds can results in about 3 meters in pseudorange measurement (Polland, 2009). The equation 2.6 shows the corrections of the satellite broadcasted time (Wells, 1999).

$$dt = a_0 + a_1(t - t_0) + a_2(t - t_0)^2 \quad 2.6$$

Where t_0 and t denote respectively the reference and current epoch, the terms a_0 , a_1 and a_2 denote respectively the satellite clock time offset, the fractional frequency offset, and the fractional frequency drift.

The Master Control Station (MCS) is responsible for calculating and transmitted the clock equation coefficients for each satellite (Kaplan & Hegrat, 2006). Consequently, the satellite rebroadcast them to the user through the navigation message. The IGS provides to GNSS users with different clock products. Those products can be used in real-time or post-process. Table 2.1 shows different clock products available on the IGS platform.

Table 2-1 IGS Clock products (The International GNSS Service, 2013)

Type	Accuracy	Latency	Updates	Sample Interval
Broadcast	~5 ns RMS	real-time	--	daily
	~2.5 ns SDev			
Ultra-Rapid (predicted half)	~3 ns RMS	real-time	at 03, 09, 15, 21 UTC	15 min
	~1.5 ns SDev			
Ultra-Rapid (observed half)	~150 ps RMS	3 - 9 hours	at 03, 09, 15, 21 UTC	15 min
	~50 ps SDev			
Rapid	~75 ps RMS	17 - 41 hours	at 17 UTC daily	15 min
	~25 ps SDev			5 min
Final	~75 ps RMS	12 - 18 days	every Thursday	15 min
	~20 ps SDev			Sat.: 30s
				Stn.: 5 min

2.5.2 Satellite orbital errors

The MCS in a process called orbital determination responsible for calculating and predicting the trajectories for all satellites. Subsequently, the prediction of satellite location is broadcasted to the user through the navigation message. Alternatively or

additionally, the IGS provides orbital corrections to the user, and Table 2.2 illustrates different orbits products available through the IGS platform.

The satellite location information is known as Ephemeris. The Ephemeris information is suffering from some errors due to environmental conditions such as atmospheric drag, additionally variation of gravitational force caused by Sun, moon, and earth; that's results in orbital variations. The errors describe satellite location can be categorized into three different categories radial, along-track, and cross-track. Figure 2.4 shows depict those errors (Wells, 1999).

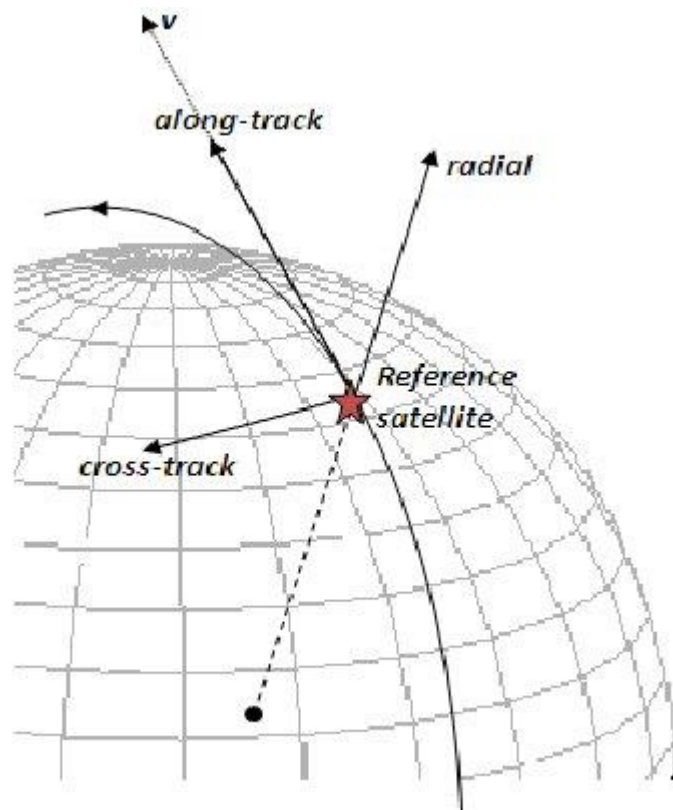


Figure 2-4 Along-track, cross-track and radial orbital components(Sundaramoorthy, Gill, Verhoeven, & Bouwmeester, 2010)

Table 2-2 IGS Orbit products (The International GNSS Service, 2013)

Type	Accuracy	Latency	Updates	Sample Interval
Broadcast	~100 cm	real-time	--	daily
Ultra-Rapid (predicted half)	~5 cm	real time	at 03, 09, 15, 21 UTC	15 min
Ultra-Rapid (observed half)	~3 cm	3 - 9 hours	at 03, 09, 15, 21 UTC	15 min
Rapid	~2.5 cm	17 - 41 hours	at 17 UTC daily	15 min
Final	~2.5 cm	12 - 18 days	every Thursday	15 min
				Stn.: 5 min

2.5.3 Satellite and receiver phase wind-up error

The satellite geometry changes to maintain the orientation of solar panels and antenna in the direction of the sun. Thus measuring the carrier phase depends on the orientation of both satellite and receiver antenna. The magnitude of one cycle affects the measuring carrier phase. This error called phase wind-up, and it mitigated through the differential GNSS techniques and PPP software (Kouba & Héroux, 2001; Wu, Wu, Hajj, Bertiger, & Lichten, 1992). The phase variation due to satellite geometry change has no impact on code measurement. Adjustment of the wind-up error is recommended for high accuracy GNSS applications (Sanz Subirana, 2013).

2.5.4 Satellite's antenna phase center error

The offset between the GNSS Satellites Mass Centre (MC) and Antenna Phase Centre (APC) results in the satellite antenna phase center error. The IGS disseminate precise satellites orbits and clock products with respect to the MC (Sanz Subirana, 2013). While the APC is broadcasted through the navigation message. (Kouba & Héroux, 2001) Consequently, the GNSS users need to adjust this offset when they use precise orbits and clock products. Figure 2.5 illustrates the offset between the center of mass and antenna phase. Since 2006 IGS has been linked the Standard Product #3 (SP3) with ANTEX files to correct the Antenna phase center (Sanz Subirana, 2013).

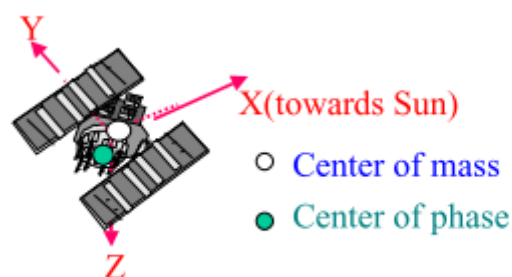


Figure 2-5 IGS conventional Antenna Phase Center in Satellite Fixed reference frame (Kouba & Héroux, 2001)

2.5.5 Receiver antenna phase center and variation error

The elevation angle, frequency, and azimuth of the arrival signal cause variation between the receiver geometry center and antenna phase center. A correction for this offset can be found in the IGS ANTEX files or with information provides by the receiver manufacturing sheet. IGS by 2006 approve the relative absolute antenna phase

center (Schmid, Steigenberger, & Gendt, 2007). Additional information about calibration factors can be found in the National Geodetic Survey website (National Geodetic Survey, 2019). Figure 2.6 illustrates the location of the antenna phase center and the receiver geometry center (Sanz Subirana, 2013).

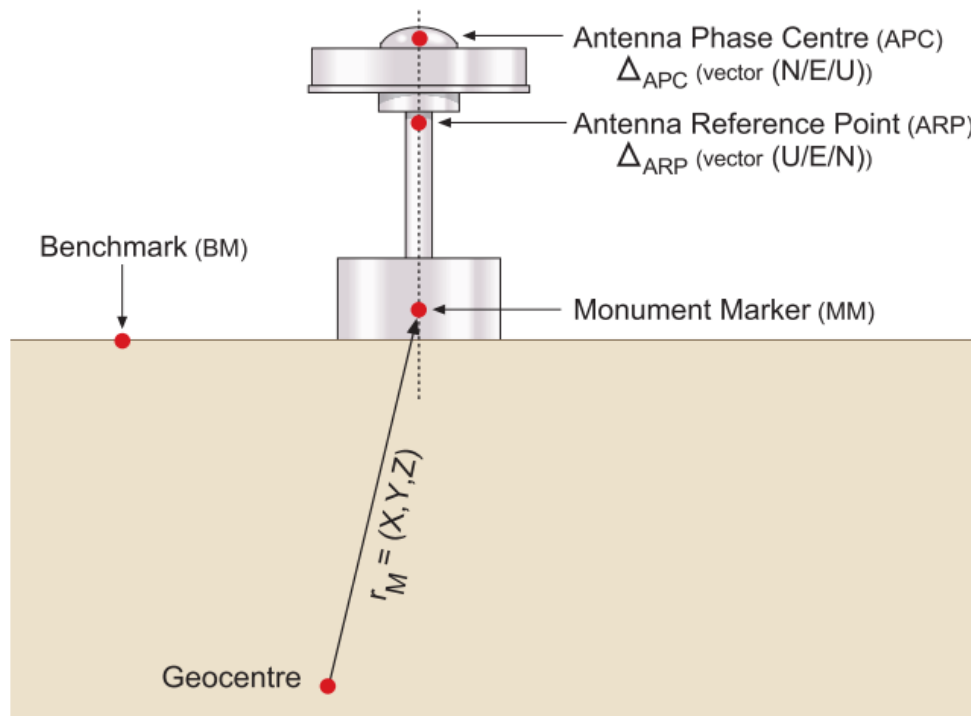


Figure 2-6 Receiver and monument centers (Sanz Subirana, 2013)

2.5.6 Receiver Clock error

The GNSS receivers are equipped with an inexpensive crystal clock to reduce the manufacturing expenses. Those clocks are less precise and accurate than those deployed in GNSS satellites (El-Rabbany, 2002). The receiver clock is suffering from noise, frequency drift, and bias (Wells, 1999). Receiver clock error is an additional unknown, and it can be solved using code or phase equations; additionally, applying ambiguity resolution with triple frequency can mitigate this error.

2.5.7 Multipath error

The code and phase measurement represents the direct measurement between the satellite and the user. The arrival signal could arrive at the GNSS receivers through direct or indirect paths (Enge & Misra, 2011). Signals arrive at the receiver through indirect paths due to reflection for obstacles like skyscrapers, buildings, or water

bodies (Wells, 1999). The multipath error disturbs both code and phase measurements (Kaplan & Hegrat, 2006). Reducing the effect of the multipath error can be done through carefully picking the GNSS stations or by using a good quality receiver antenna, which is an additional solution for reducing multipath errors (B.Hoffmann-Wellenhof & H.Lichtenegg, 2001; Polland, 2009). Figure 2.7 shows direct and indirect paths for the satellite signal.

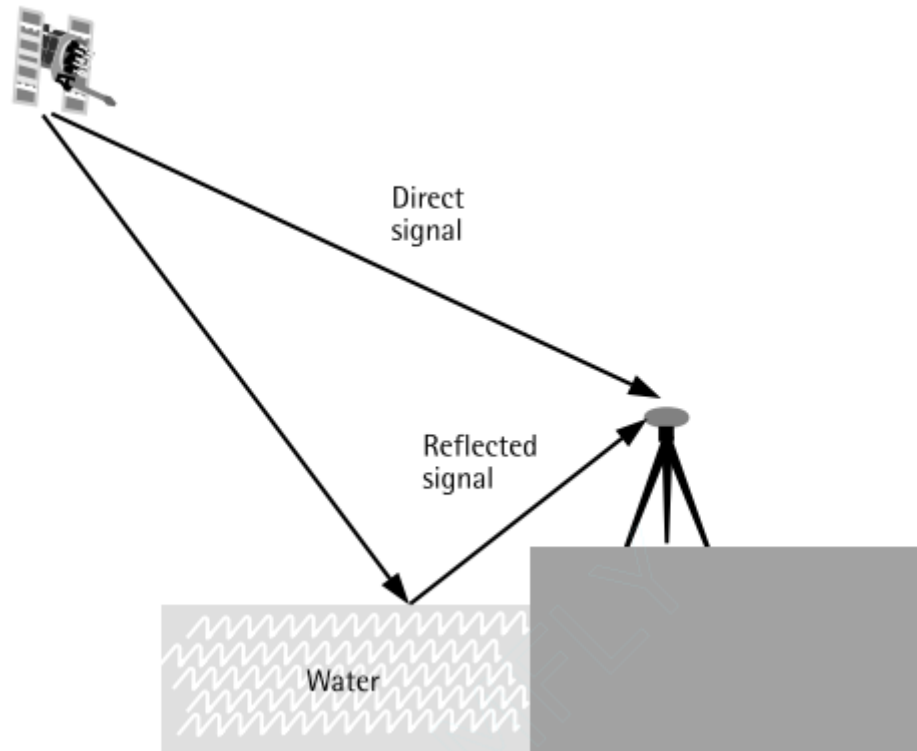


Figure 2-7 Multipath Error (El-Rabbany, 2002)

2.5.8 Atmospheric error

The earth's atmosphere consists of several layers. The variation of temperature defines the border between the adjacent layers (Noël, 2012). Through the signals journey from satellite to the earth, the signals exposed to travel through different layers. This affects the GNSS signals to exposed delay; the speed of the signals is slowing down and bending due to the variation of the atmospheric refractive index (Dodson, 1986; Sanz Subirana, 2013). The ionosphere and troposphere have a major influence on GNSS signals (El-Rabbany, 2002). Figure 2.8 shows the extent of both layers.

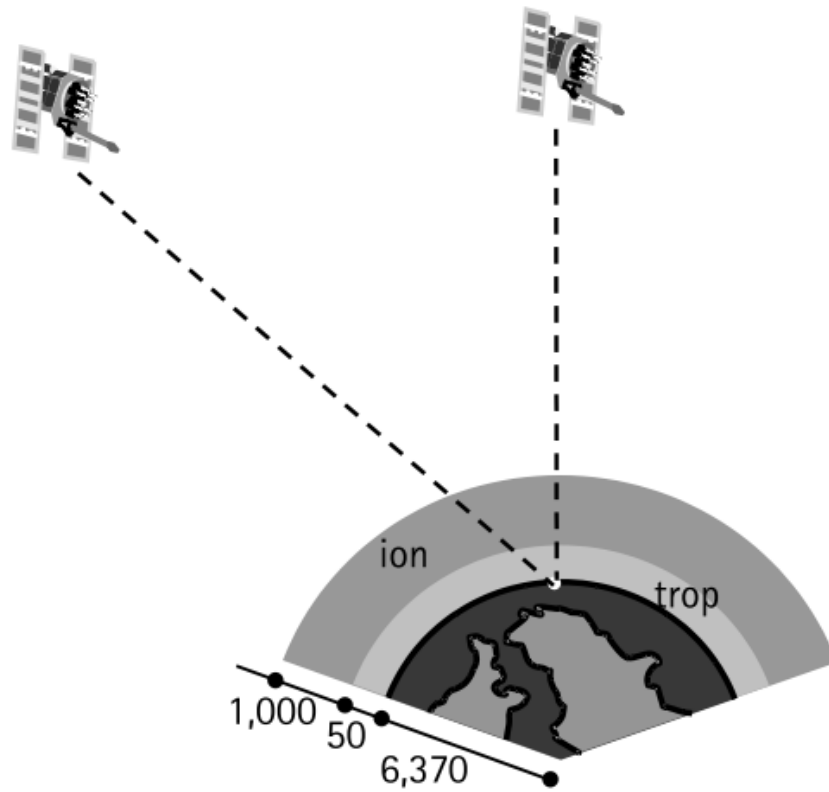


Figure 2-8 Ionosphere and troposphere layer

2.5.9 Ionosphere error

The Ionospheric layer lay from 50 to 1000 km above the earth's surface. The interaction between atmospheric molecules and electromagnetic radiation takes place in this layer (El-Rabbany, 2002). Consequently, the ionization interaction release positive and negative charges (Sanz Subirana, 2013). The influence of free negative charges, which denoted as Total Electron Content (TEC). (B. Hoffmann-Wellenhof & H.Lichtenegg, 2001) Defined TEC as “The total electron content along the signal path between the satellite and the receiver.” TEC impacts both the speed and the path of the coming GNSS signals. The phase refractive index n_{ph} and the group refractive index n_{gr} , can be determined by the equations 2.7 and 2.8.

$$n_{ph} = 1 - \frac{40.3}{f^2} * N_e \quad 2.7$$

$$n_{gr} = 1 + \frac{40.3}{f^2} * N_e \quad 2.8$$

Where N_e denote the electron density in (e-/m³), f represents the frequency for the GNSS signal passing through the ionospheric layers.

The ionosphere delayed code measurement and speedup the group phase velocity (El-Rabbany, 2002). Therefore the computed range between the satellite and the user experiences a range error due to ionosphere delay Δ^{Iono} (B.Hoffmann-Wellenhof & H.Lichtenegg, 2001). Δ^{Iono} value varies from 5-150 meters depending on solar activity and satellites elevation angels (Wells, 1999).

$$\Delta^{Iono} = \pm \frac{40.3}{f^2} * TEC \quad 2.9$$

Where Δ^{Iono} represents the ionospheric refraction, and TEC represents the total electron content in a defined cylindrical path construct between the satellite and user. The geographical location of the GNSS user, observation time, season, and solar flares activities affect the density of the TEC (NovAtel Inc, 2015). The ionospheric delay, as mentioned before, highly correlated to the frequency and the geographic location. Therefore the differential GNSS mitigate this error using a pair of GNSS receiver located in the same region (with 20 km baseline). Dual-frequency GNSS receivers can take advantage of the different impacts of the ionosphere on diverse frequencies (Wells, 1999). Equations 2.10 and 2.11 shows the ionosphere free combination (Sanz Subirana, 2013). While the single frequency receiver can use Klobucher model, NeQuik Model or other ionospheric corrections disseminated from a network of GNSS receivers (El-Rabbany, 2002; Sanz Subirana, 2013)

$$\varphi_{Iono-free} = \frac{f_1^2 * \varphi_1 - f_2^2 * \varphi_2}{f_1^2 - f_2^2} \quad 2.10$$

$$R_{Iono-free} = \frac{f_1^2 * R_1 - f_2^2 * R_2}{f_1^2 - f_2^2} \quad 2.11$$

Where φ denote the phase measurements, R denote the code measurements, while f represent different frequencies disseminated from the GNSS satellite.

The variation of the GNSS signals path is negligible for satellites that have 5 degrees elevation angle or more (El-Rabbany, 2002). However, satellite elevation angles must be taken into account with the Total Vertical Electron Content (TVEC). Equation 2.12 shows the relation between the ionospheric delay corresponding with TEVC and zenith angle z' (B.Hoffmann-Wellenhof & H.Lichtenegg, 2001).

$$\Delta^{Iono} = \pm \frac{1}{\cos z'} \frac{40.3}{f^2} * TVEC \quad 2.12$$

Where Δ^{iono} represents the Ionospheric delay, and $TVEC$ represents the vertical total electron content in predefined cylindrical path between the satellite and user, and z denote the zenith angle between GNSS satellite and GNSS user.

2.5.10 Troposphere error

The earth's atmosphere consists of many layers. The first layer, which is adjacent to the earth's surface, called the troposphere layer (NovAtel Inc, 2015). This layer ranges from 0-50 km (El-Rabbany, 2002). Unlike the ionosphere layer, the troposphere is a neutral medium. The troposphere affects phase and code measurements with the same amount of delay. Since it a non-dispersive medium for L band frequency, which is less than 15 GHz (Sanz Subirana, 2013). Dry and wet components affect the tropospheric delay (Wells, 1999). The refractive index of the air in equation 2.13 divide into two categories hydrostatics and wet. Oxygen and Nitrogen are examples of dry gases, while rain, cloud and water vapor are examples of a wet category (Sanz Subirana, 2013).

$$N = N_{hydr} + N_{wet} \quad 2.13$$

The tropospheric dry delay participates with 90% of the total delay, which leads to range error that could vary between 2.3 – 10 meters. While the wet delay participates with 10% of total delay with a few tens of centimeters (Sanz Subirana, 2013; Wells, 1999).The amount of tropospheric delay depends on many factors such as atmospheric pressure, temperature, Humidity, satellite zenith angle, and receiver height above the sea level (Wells, 1999). The ionosphere free combination cannot mitigate the tropospheric delay as the tropospheric delay impact both frequencies with the same amount (Sanz Subirana, 2013). As a matter of fact, the differential GNSS can mitigate tropospheric delay with a realistic amount, especially if the weather conditions along the baseline are identical. Many models provide corrections for the tropospheric delay. The Hopfield, Mapping of Niell, Saastamoinen model, and other models used to mitigate tropospheric error (B.Hoffmann-Wellenhof & H.Lichtenegg, 2001; Niell, 1996). All the GNSS errors are summarized in Figure 2.9.

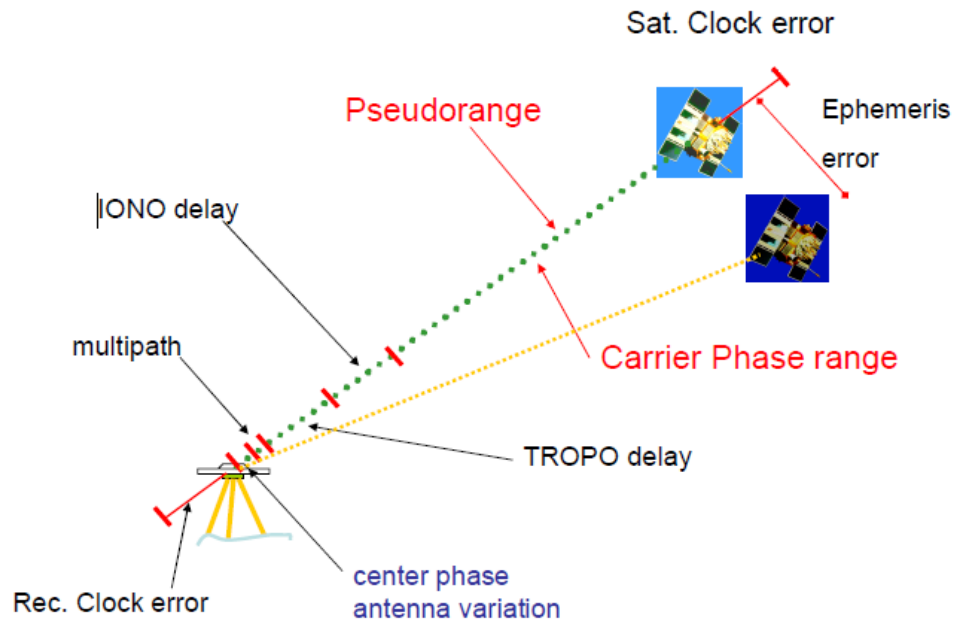


Figure 2-9 Overview of GNSS errors

2.6 Precise Point Positioning

Determining position with centimeters level of accuracy can be achieved using differential GNSS methods such as statics and RTK; which, mitigating the common errors along the baseline by using two or more receivers (local GNSS networks). To reach the same accuracy level on a global scale using only a single receiver, it is necessary first to use The International Terrestrial Reference Frame (ITRF) to determine the coordinates globally (International Earth Rotation and Reference System Service, 2013). Thus the crustal deformation, variation of coordinates due to the sun and moon gravitational force, ocean tides, atmospheric pressure, and snow cover have been implemented in the ITRF. More about ITRF and ITRF correction models can be found in (Kouba & Héroux, 2001). Secondly, it is essential to provide GNSS users with corrections through internet links or satellite communications (Engel & Misra, 2011). Those corrections are calculated and disseminated by global GNSS networks such as IGS. Through Networked Transport of RTCM via Internet Protocol (Weber et al., 2005), IGS provides the RTS to the GNSS users, RTS disseminating as RTCM State-Space Representation (SSR) correction streams (RTCM

Special Committee, 2016). The following equations describe the computational method of PPP in real-time.

1. The range and phase Iono-Free equations 2.10 and 2.11 used to determine the pseudorange.
2. The corrections in RTCM_SSR are divided into three categories. The first category concerns to radial, along-track, and cross-track corrections for the satellites' locations. The second category of corrections is concerned about the rate of correction for radial, along-track, and cross-track. The last category uses to solve the satellite clock's biases.

$$\Delta_{ssr}(t_0, IODE) = (\delta O_r, \delta O_a, \delta O_c; \delta O'_r, \delta O'_a, \delta O'_c; C_0, C_1, C_2) \quad 2.14$$

Where δO_r , δO_a and δO_c are the correction components in radial, along-track, and cross-track directions respectively, $\delta O'_r$, $\delta O'_a$, $\delta O'_c$ denote the correction rates respectively in radial, along-track, and cross-track directions, C_0 , C_1 , C_2 terms are the polynomial coefficient terms of real-time satellite clock corrections.

3. The Transformation of the satellite corrections from orbital coordinates to Earth Center Earth Fixed (ECEF) coordinates systems.

$$\delta X_t \equiv \begin{bmatrix} \delta x \\ \delta y \\ \delta z \end{bmatrix} = R \cdot \begin{bmatrix} \delta O_r \\ \delta O_a \\ \delta O_c \end{bmatrix} \quad 2.15$$

Where δx , δy , δz are the correction components in the X, Y, and Z directions for epoch t.

4. The corrections of the broadcasted satellites coordinates:

The corrections (δx , δy , δz) from the last step will add to the broadcasted satellite coordinates.

$$\begin{bmatrix} X_{prec} \\ Y_{prec} \\ Z_{prec} \end{bmatrix} = \begin{bmatrix} X_{brdc} \\ Y_{brdc} \\ Z_{brdc} \end{bmatrix} - \begin{bmatrix} \delta x \\ \delta y \\ \delta z \end{bmatrix} \quad 2.16$$

5. The corrections of broadcasted satellites time:

The transmitted and receiving times are very crucial for navigation solutions to correct the broadcasting time. The following equation shows the formula used to correct the broadcasting time.

$$tsprec = tsbrdc - \delta Cc \quad 2.17$$

$$\delta Cc = C_0 + C_1(t - t_0) + C_2(t - t_0)^2 \quad 2.18$$

Where $tsprec$ denote the precise satellite time, and $tsbrdc$ denote the broadcasted satellites time, while δC is the corrections of satellites time depending on the coefficients C_0 , C_1 , and C_2 .

2.7 Machine learning

Machine learning, Artificial Intelligent, and deep learning are involved more and more in our daily life. Learning from the data, data understanding, and data visualization is essential for better data modeling, data classification, and prediction. Machine learning is used to solve many problems in GNSS domain such as multipath detection, predicting troposphere and ionosphere and others (Dong et al., 2018; Hsu, 2017; Sánchez-Naranjo, González, Ramos-Pollán, & Solé, 2016; Shamshiri, Motagh, Nahavandchi, Haghshenas Haghghi, & Hoseini, 2020). This section shows the theoretical background for the Support Vector Machine and RandomForest.

2.7.1 Support Vector Machine (SVM)

The SVM is considered as the most successful method in machine learning due to the conventional formulation and simple formation (Clarkson, Hazan, & Woodruff, 2012). The SVM is used to expand the Support Vector Classifier (SVC) to adapt to a higher-dimensional space (Parang, Wiebe, & Knaus, 2012). The kernel trick is using to transform the data into a higher separable dimensional space. Different examples of the kernel, such as polynomial, Radial Base Function (RBF), and others can find in (I. Guyon, B. Boser, & V. Vapnik, 1993). Giving a data set contains $\{(x_i, y_i, i = 1, 2, \dots, m)\}$ where $x_i \in R^n$ and the label are $y_i \in (+1, -1)$. SVC define the hyperplane “In a p-dimensional space, a hyper plane is a flat affine surface of dimensional P-1”. Figure 2.10 shows the hyperplane separate a two dataset (Parang et al., 2012).

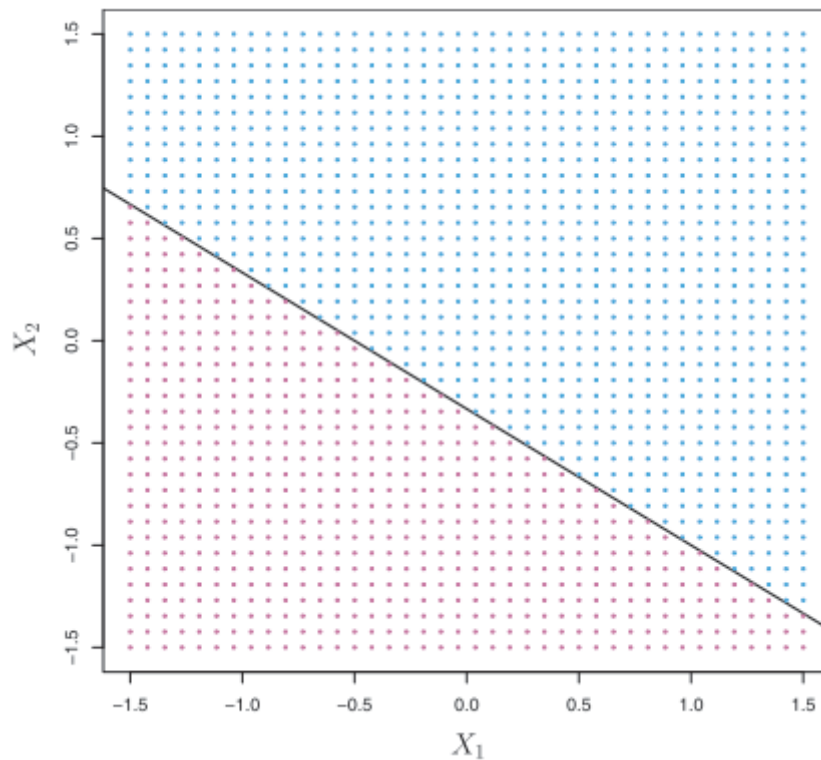


Figure 2-10 The solid black line defined the hyperplane separated the two classes of data(Parang et al., 2012)

In reality, many hyperplanes can be used to classify any datasets. (I. Guyon et al., 1993) introduced the idea of defining a hyperplane with maximal margin using only a few amounts of data near to the hyperplane surface, which called the support vectors (Kumar, Bhattacharyya, & Gupta, 2014). Figure 2.11 shows the support vectors and maximal margin hyperplane.

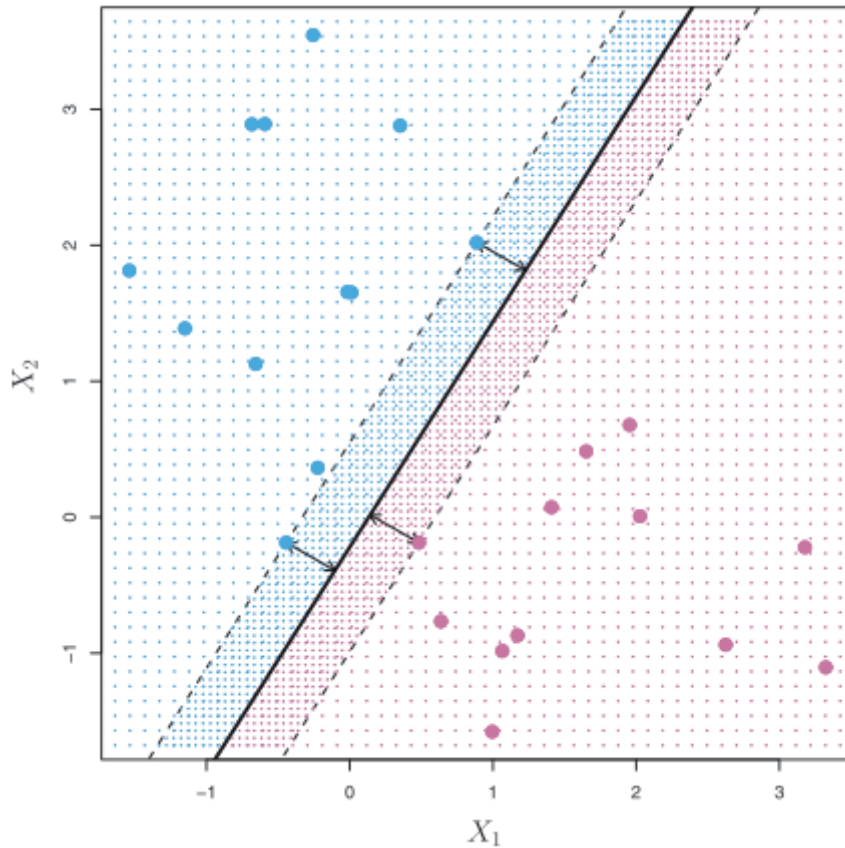


Figure 2-11 The support vectors use for maximal margin hyperplane (Parang et al., 2012)
 The formulation equation describes the soft margin SVM are given by (SMOLA, 2004):

$$\text{minimize}_{w,b,\xi} = \frac{1}{2} w^T w + C \sum_{i=1}^m \xi_i \quad 2.19$$

Subjected to $y_i(w^T x_i + b) \geq 1 - \xi_i, \xi_i \geq 0, \text{ for } 1 \leq i \leq m$

Where w denote the width of the margin, b denote the bias, ξ denote the slack variable allowing some instant or blunders to fall in the margin, and C denote the trade-off margin width.

2.7.2 Decision Tree and RandomForest

Solving classification and regression problems can be done using many machine learning methods. Classification and Regression Tree, also known as (CART), is a supervised machine learning. The decision tree draw upside down where the roots up and the leaves are down. Containing different parts edges, root, and terminal nodes or leaves (Quinlan, 1986). Data prediction for continuous variables done by calculating the mean, while for categorical problems, it has been done by calculating the mode (Parang et al., 2012). The mathematical idea behind the decision tree is to split the data

into different classes. Consequently, this splitting minimized the Residual Sum of Squares (RSS) and increased the gain of information from that class.

For data $X_1, X_2, X_3, \dots, X_p$ are split into different regions $R_1, R_2, R_3, \dots, R_J$

The aim is to construct different classes that minimize RSS

$$\sum_{j=1}^J \sum_{i \in R_j} (y_i - \hat{y}_{R_j})^2 \quad 2.20$$

Increasing the random splitting regions will lead to having more homogeneous groups of data, while this can lead to overfitting problems. (Buntine & Niblett, 1992) concluded that random splitting is not improving classification precision. Pruning and bagging have been used in construction decision trees to reduce the variances (Parang et al., 2012).

The Random Forest is a way to improve the execution off single tree decisions. The sample with replacement techniques used to build different trees. In other words, each time a decision tree needs to build by using a different random sample from the original dataset (Breiman, 2001). Consequently, highly decorrelated trees will create, thus, a significant reduction in variance (Parang et al., 2012). The RandomForest can use as decision trees for both classification and regression problems (Breiman, 2001).

2.7.3 Cross-Validation (CV) and GridSearchCV

The CV is the way to test machine learning classification or regression. To perform an un-bias test, the original data has to split into the train and test dataset. Different validation algorithms have been developed to perform CV (Parang et al., 2012). However, the general procedures for those algorithms firstly are to fit the model by using the train data.

Consequently, the model created from the fitting phase used to classify the test data in classification problems. While for non-categorical data, the model created in the fitting phase is used as a Regressor. Different metrics such as confusion matrix are used to evaluate the ability of the model to classify the test data well, while the Root Means Squared error (RMS) is a matrix use to evaluate models for continuous data.

Figure 2.11 shows the maximum margin can be defined to separate the blue and purple datasets. This figure shows the hard margin SVM when the margin constructs without adapting any errors. Where the soft margin SVM, which shows in equation 2.19, has the term C and ξ to adapt permitting of errors. Thus the SVM allows some violation.

Due to the reasonability of adapting violation of some points. Thus the margin does not shrink to adapt all the points (Awad & Khanna, 2015). Figure 2.12 illustrates the concept of hard and soft margin.

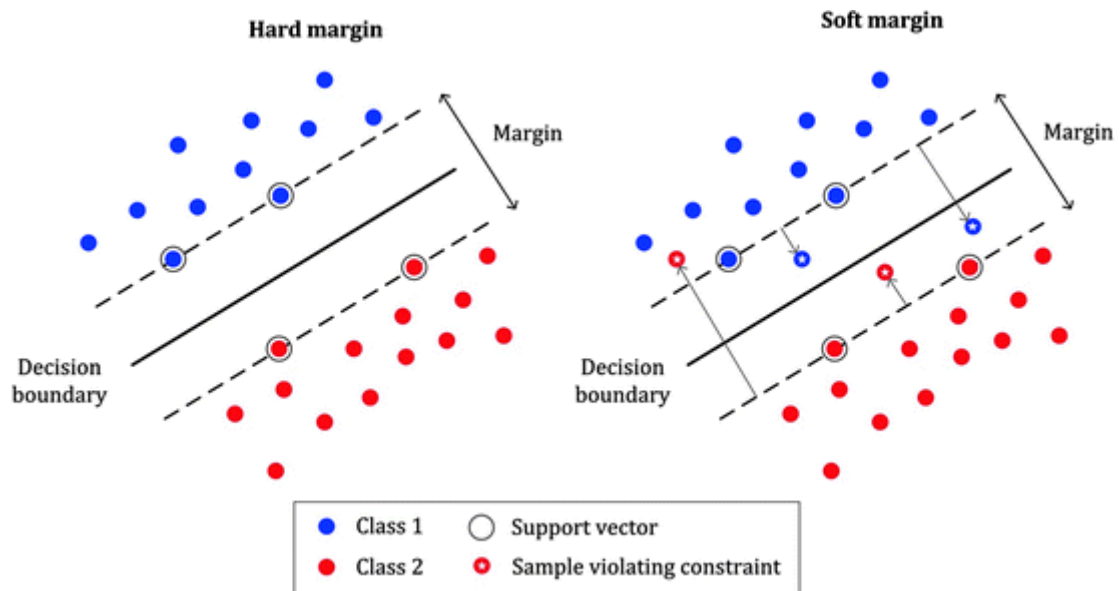


Figure 2-12 SVM margin (“Math behind SVM(Support Vector Machine),” 2019)

The use of the kernel trick aids in making the data more separable. In this research, the RBF used as a kernel for SVM. Consequently, it essential to tune the parameters for this kernel. The gamma γ parameter plays a major role in interpolating, extrapolating, and define the Gaussian shape (Mongillo, 2011).

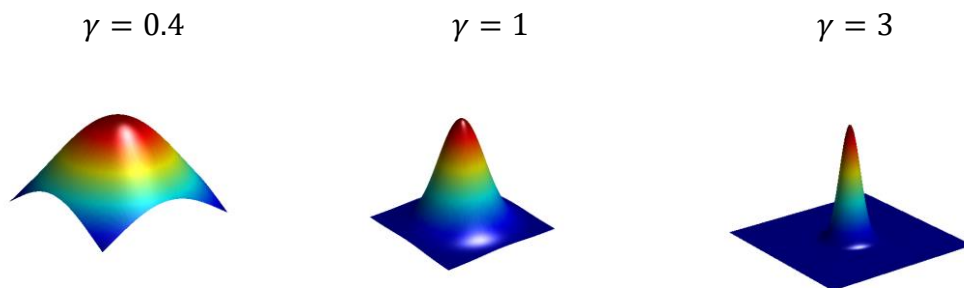


Figure 2-13 Effect of using different values of gamma (Mongillo, 2011)

As it mentions, the gamma and C values controlling the SVR, thus to conclude, C controls the cost of misclassification. Consequently, a large C value gives low bias and high variance. On the contrary, small C, values give a higher bias with low variance. While small values of gamma for RBF means have a wide Gaussian shape with high

bias and low variance. And on the contrary, the small gamma value sharpens the edges of the Gaussian, and that leads to low bias and high variance (Parang et al., 2012).

The RF as the SVR has many parameters to tune, such as the forest trees number, the maximum number of features to allow the node to split, the maximum depth for defining how much the tree should grow, and the method of sampling and replacement. More about the RandomForest parameters can be found in (Scornet, 2017).

Finally, there is no such way to define the parameters for all regression and classification cases. Thus the GridSearchCV for both RandomForest and Support Vector Machine has been used for parameter tuning. Different values are assigned randomly for those parameters. Consequently, the outcome error from different combinations is calculated. GridSearchCV assigns a high score for those combinations that result in the minimum amount of error. The recommendation from the machine learning community is to refine the parameters through multiple iterations.

2.8 BNC Software overview

The BNC is an open-source program developed by Bundesamt für Kartographie und Geodäsie (BKG). Different setup versions are available to download for different operating systems <https://igs.bkg.bund.de/ntrip/download>. The BNC is mainly used for real-time, and post-process GNSS data streams through NTRIP (Weber et al., 2005). The BNC works with data streaming coming from EUREF, MGEX, IGS, and other GNSS networks. BNC contains many tools such as the SP3 comparison tool; the SP3 file contains satellite orbital information. Broadcast correction tools are mainly used to store and read correction files disseminated from different analysis centers. PPP tools are used for real-time and post-process GNSS data, and Receiver Independent Exchange Format (RINEX) converting tool. Figure 2.14 shows different BNC tools (Georg Weber, Leoš Mervart, Andrea Stürze, Axel Rülke & Stöcker, 2016).

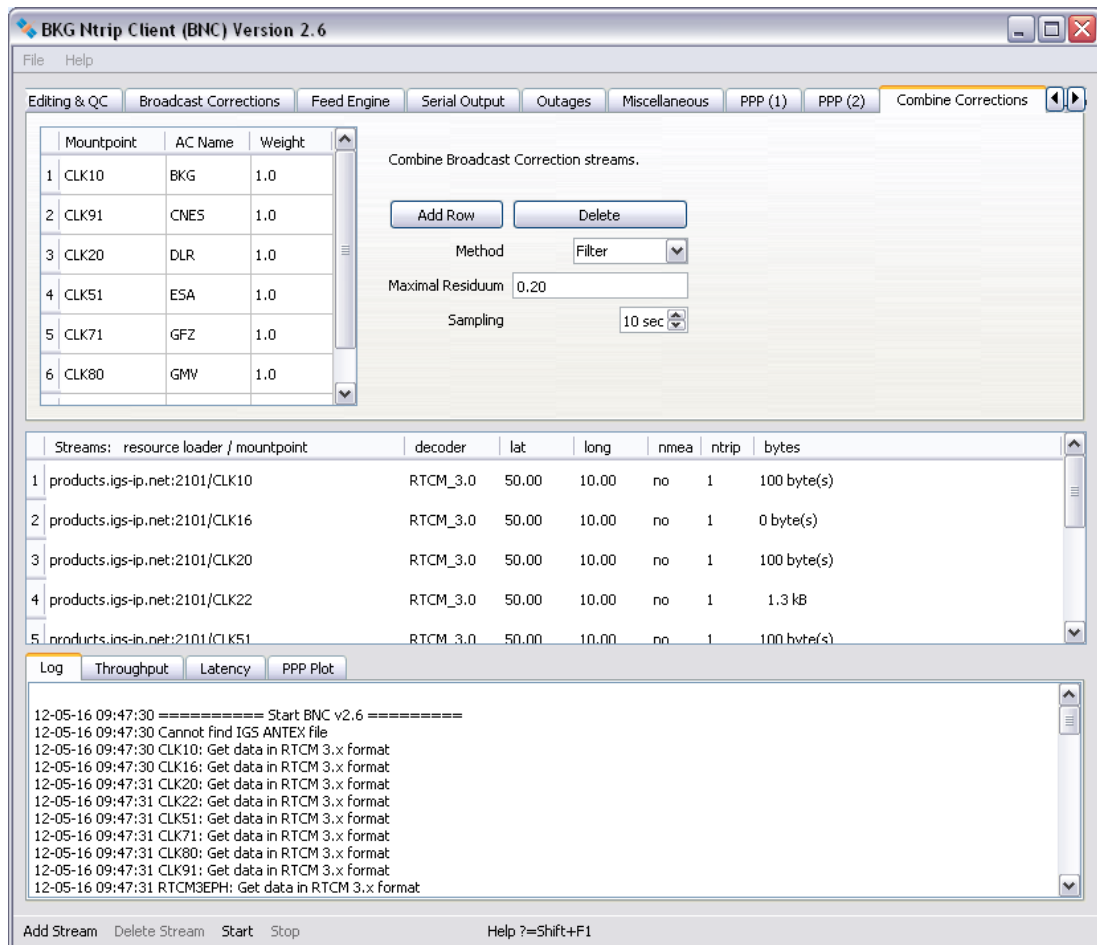


Figure 2-14 BNC Software interface (Georg Weber, Leoš Mervart , Andrea Stürze , Axel Rülke & Stöcker, 2016)

2.9 Python and complementary libraries

Understanding the capability of python libraries. In fact, there are numbers of libraries, which can be used to deal with massive data, prediction, data visualizing, and data classification. For example, Matplotlib, Seaborn, and Plotly are dedicated to data visualization. Pandas and Numpy deal with math functions and series analysis. SciKit-learn library for machine learning in python software (Matplotlib, 2012; Plotly, 2018; python organization, 2016; SciKit-Learn, 2016; Seaborn, 2012).

Chapter 3 Research Methodology

This chapter presents the method carried out in this research. The work in this research organized in different Work Packages (WP), which is designed to cover all different steps performed on this research, this chapter contains two methodologies, and the first one represents different steps performed to assess the performance of different SVR kernels. The second methodology represents different steps implemented to perform the real-time simulation for a GNSS user. The first methodology includes the SVR method, while the second methodology includes the SVR and the RF. Followed by statistical assessments investigated the performance of the applied machine learning tools.

3.1 WP1 General reviewing

3.1.1 Literature Review

In this research, the literature review includes a review of related studies and researches on the PPP field, including the different evaluation and assessment of clock and orbital products. Investigations about the current accuracy achieved using real-time PPP. A review of the different sources of errors affects the GNSS system. Consequently, an investigation of various methods applies to error mitigation. Explained the significance and importance of solving the latency problem. The first work package includes a review of BNC software as a tool for solving real-time PPP. After that, a search and review of machine learning prediction models as a tool for solving latency problems.

3.2 WP2 IGS products and stations

3.2.1 IGS Brest station

Currently, The IGS operates and tracks around 500 stations. The Brest station in France is piked as it provides an RTS stream for real-time PPP. Nowadays, The Brest station is operating with Trimble 57971 receiver. More information about the Brest station can found in the log file on the [IGS website](#). In fact, the applied methodology in this research applies to any station that provides real-time data streaming. Figures 3.1 and 3.2 show the receiver mount point in Brest and the location of Brest station,

respectively (IGS, 2020). Table 3.1 shows the polar and Cartesian ITRF coordinates of Brest station.

Table 3-1 Brest coordinates (IGS, 2020)

Coordinates components	Coordinates values
X coordinate (m)	4231162.000
Y coordinate (m)	-332747.000
Z coordinate (m)	4745131.000
Latitude (N is +)	+482249.79
Longitude (E is +)	-0042947.76
Elevation (m,ellips.)	65.5



Figure 3-1 Brest station receiver mount point(IGS, 2020)

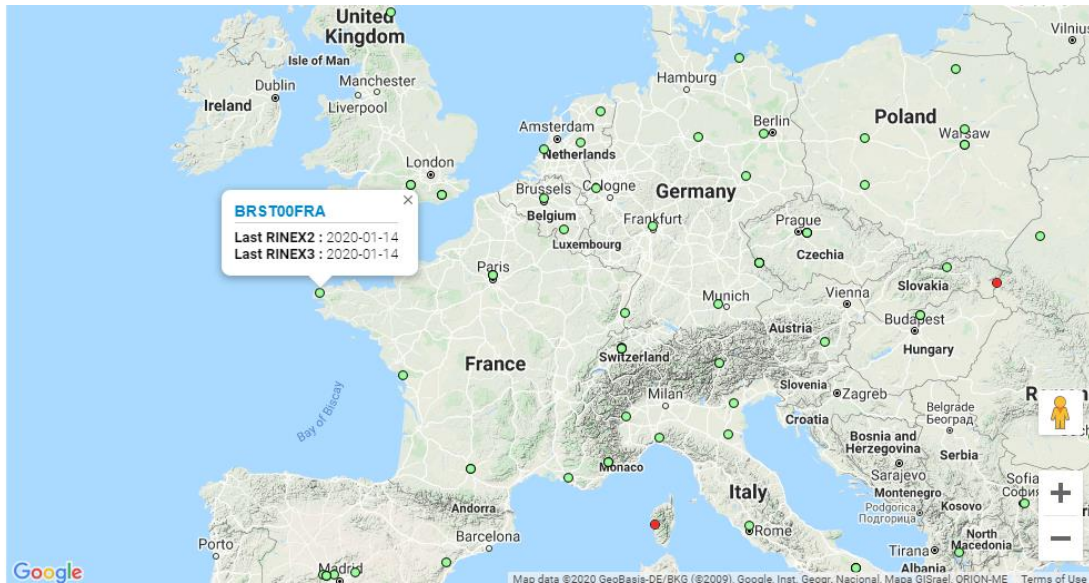


Figure 3-2 Brest station location(IGS, 2020)

3.2.2 Products and Analysis centers

In this research The CLK11 and IGS03 correction files used as RTS streams, German Aerospace Center (DLR) provide a CLK11; CLK11 contains the orbital, clock, and code bias corrections for both GLONASS and GPS. While, IGS03 which is a combined product from different analysis centers, provide orbital and clock corrections for GLONASS and GPS.

3.3 WP3 Data preparation

3.3.1 Data cleaning

In this phase, pandas, numpy, and python are used to read the correction files. Consequently, the clock corrections with the timestamp for each satellite are added to the numpy array. Then, the numpy array was converted to the pandas data frame. The final output of this phase is two data frames; one for CLK11 and the other for IGS03. The resulted CLK data Frame contains 52 columns with 51774 rows. However, the IGS03 data Frame contains 52 columns with 25881 rows. In fact, the difference in rows number is due to different sampling intervals, which is 10 seconds in the IGS03 while it is 5 seconds in the CLK11. Each data frame contains the time stamp as an index, and each column represents the clock corrections belong to one satellite. Figures 3.3 and Table 3.2 shows the original text file and the final data frame for CLK11 product. Where letter G indicates the GPS satellite and letter R indicates the GLONASS satellite.

```

171 > CLOCK 2019 12 13 09 26 00.0 2 49 CLK11
172 G01 53 2.5617 0.0000 0.0000
173 G02 52 2.1467 0.0000 0.0000
174 G03 66 1.0111 0.0000 0.0000
175 G05 36 2.0091 0.0000 0.0000
176 G06 72 1.2763 0.0000 0.0000
177 G07 103 1.9060 0.0000 0.0000
178 G08 42 2.0612 0.0000 0.0000
179 G09 93 0.9090 0.0000 0.0000
180 G10 53 0.1624 0.0000 0.0000
181 G11 19 0.7776 0.0000 0.0000
182 G12 8 -0.1547 0.0000 0.0000
183 G13 29 3.2501 0.0000 0.0000
184 G14 64 1.0067 0.0000 0.0000
185 G15 102 0.1414 0.0000 0.0000
186 G16 67 2.0396 0.0000 0.0000
187 G17 30 -3.0189 0.0000 0.0000
188 G19 65 -1.1761 0.0000 0.0000
189 G20 60 2.5875 0.0000 0.0000
190 G21 62 1.9635 0.0000 0.0000
191 G22 12 0.0647 0.0000 0.0000
192 G23 35 1.7500 0.0000 0.0000
193 G24 42 0.1812 0.0000 0.0000
194 G25 29 1.1841 0.0000 0.0000
195 G27 30 0.5053 0.0000 0.0000
196 G28 35 -0.7208 0.0000 0.0000
197 G29 80 -0.5155 0.0000 0.0000
198 G30 105 -0.2917 0.0000 0.0000
199 G31 51 1.3039 0.0000 0.0000
200 G32 62 1.3791 0.0000 0.0000

```

Figure 3-3 CLK11 text file CLK11

Table 3-2 sample of the data in the created CLK data frame

	G01	G02	R01	R02	Ticks
13/12/2019 09:26:00	2.5617	2.1467	3.9201	1.4676	0
13/12/2019 09:26:05	2.5597	2.15	3.9271	1.4574	1
13/12/2019 09:26:10	2.5597	2.1498	3.9162	1.465	2
13/12/2019 09:26:15	2.5587	2.1495	3.9132	1.4399	3

3.3.2 Data Preparation

The choice of downloading the latency information was enabled during the PPP; the BNC software in this phase creates a text file that contains the solved coordinate's values of Brest station. Simultaneously, the BNC software recorded the latency values during the implementation of real-time PPP. Consequently, a bunch of python code lines is used to add that information to the main data frame. It is worth to mention here a different sampling interval of written the latency values used by BNC. Thus, to keep consistency, the latency values rounded to the nearest 5 seconds in the CLK data frame, while the 10 seconds rounded values are used on the case of the IGS03 data frame. Figure 3.4 and Table 3.3 show the original text file contains latency information, and the field contains the latency information in the final data frame.

```

10335 19-12-14 02:24:22 2019-12-14_02:24:22.000 BRST00FRAO X = 4231163.7304 Y = -332746.5165 Z = 4745132.0996 NEU: +0.00
10336 19-12-14 02:24:23 2019-12-14_02:24:23.000 BRST00FRAO X = 4231163.7291 Y = -332746.5186 Z = 4745132.1029 NEU: +0.00
10337 19-12-14 02:24:24 2019-12-14_02:24:24.000 BRST00FRAO X = 4231163.7200 Y = -332746.5189 Z = 4745132.0952 NEU: +0.00
10338 19-12-14 02:24:25 2019-12-14_02:24:25.000 BRST00FRAO X = 4231163.7255 Y = -332746.5161 Z = 4745132.1015 NEU: +0.00
10339 19-12-14 02:24:26 2019-12-14_02:24:26.000 BRST00FRAO X = 4231163.7145 Y = -332746.5226 Z = 4745132.0900 NEU: +0.00
10340 19-12-14 02:24:27 CLK11 Clock: Mean latency 7.29 sec, min 7.19, max 7.39, rms 0.09, 2 epochs, 0 gaps
10341 19-12-14 02:24:27 CLK11 CodeBiases: Mean latency 7.29 sec, min 7.19, max 7.39, rms 0.09, 2 epochs, 0 gaps
10342 19-12-14 02:24:27 2019-12-14_02:24:27.000 BRST00FRAO X = 4231163.7270 Y = -332746.5150 Z = 4745132.1061 NEU: +0.00
10343 19-12-14 02:24:28 2019-12-14_02:24:28.000 BRST00FRAO X = 4231163.7251 Y = -332746.5160 Z = 4745132.0973 NEU: +0.00
10344 19-12-14 02:24:29 2019-12-14_02:24:29.000 BRST00FRAO X = 4231163.7201 Y = -332746.5153 Z = 4745132.0960 NEU: +0.00
10345 19-12-14 02:24:30 2019-12-14_02:24:30.000 BRST00FRAO X = 4231163.7154 Y = -332746.5151 Z = 4745132.0797 NEU: +0.00
10346 19-12-14 02:24:31 2019-12-14_02:24:31.000 BRST00FRAO X = 4231163.7414 Y = -332746.5149 Z = 4745132.1022 NEU: +0.00
10347 19-12-14 02:24:32 2019-12-14_02:24:32.000 BRST00FRAO X = 4231163.7355 Y = -332746.5186 Z = 4745132.0958 NEU: +0.00
10348 19-12-14 02:24:33 2019-12-14_02:24:33.000 BRST00FRAO X = 4231163.7192 Y = -332746.5221 Z = 4745132.0899 NEU: +0.00
10349 19-12-14 02:24:34 2019-12-14_02:24:34.000 BRST00FRAO X = 4231163.7222 Y = -332746.5214 Z = 4745132.0905 NEU: +0.00
10350 19-12-14 02:24:35 2019-12-14_02:24:35.000 BRST00FRAO X = 4231163.7204 Y = -332746.5206 Z = 4745132.0892 NEU: +0.00
10351 19-12-14 02:24:36 2019-12-14_02:24:36.000 BRST00FRAO X = 4231163.7183 Y = -332746.5211 Z = 4745132.0924 NEU: +0.00
10352 19-12-14 02:24:37 CLK11 Clock: Mean latency 6.9 sec, min 6.61, max 7.19, rms 0.29, 2 epochs, 0 gaps
10353 19-12-14 02:24:37 CLK11 CodeBiases: Mean latency 6.9 sec, min 6.61, max 7.19, rms 0.29, 2 epochs, 0 gaps
10354 19-12-14 02:24:37 2019-12-14_02:24:37.000 BRST00FRAO X = 4231163.7380 Y = -332746.5156 Z = 4745132.0982 NEU: +0.00
10355 19-12-14 02:24:38 2019-12-14_02:24:38.000 BRST00FRAO X = 4231163.7326 Y = -332746.5201 Z = 4745132.0967 NEU: +0.00
10356 19-12-14 02:24:39 2019-12-14_02:24:39.000 BRST00FRAO X = 4231163.7156 Y = -332746.5248 Z = 4745132.0728 NEU: +0.00
10357 19-12-14 02:24:40 2019-12-14_02:24:40.000 BRST00FRAO X = 4231163.7330 Y = -332746.5196 Z = 4745132.0912 NEU: +0.00
10358 19-12-14 02:24:41 2019-12-14_02:24:41.000 BRST00FRAO X = 4231163.7261 Y = -332746.5223 Z = 4745132.0880 NEU: +0.00
10359 19-12-14 02:24:42 2019-12-14_02:24:42.000 BRST00FRAO X = 4231163.7369 Y = -332746.5165 Z = 4745132.0908 NEU: +0.00
10360 19-12-14 02:24:43 2019-12-14_02:24:43.000 BRST00FRAO X = 4231163.7348 Y = -332746.5193 Z = 4745132.0866 NEU: +0.00
10361 19-12-14 02:24:44 2019-12-14_02:24:44.000 BRST00FRAO X = 4231163.7325 Y = -332746.5159 Z = 4745132.0791 NEU: +0.00

```

Figure 3-4 CLK coordinates and latency value text file

Table 3-3 the final CLK data frame with latency values

	G01	G02	R01	R02	Ticks	final latency
13/12/2019 09:26:00	2.5617	2.1467	3.9201	1.4676	0	5
13/12/2019 09:26:05	2.5597	2.15	3.9271	1.4574	1	5
13/12/2019 09:26:10	2.5597	2.1498	3.9162	1.465	2	10

3.4 WP4 Machine learning

The fourth work package contains two main tasks; the first task is concerned about the potentiality of using the Support Vector Regression as a tool for solving the latency problem, the SVR with different kernel type is examined. However, the second phase is concerned with the simulation of real-time GNSS users. Real-time GNSS applies the SVR, or the RF as a Regressor to predict the clock corrections.

3.4.1 The potentiality of SVR in solving latency

In this phase, the BNC software was used in real-time PPP from around 9:00 o'clock on 23/10/2019 till 12:00 o'clock on 24/10/2019. The BNC produced CLK11 and IGS03 correction files. Thus an investigation of the potentiality of using SVR to overcome the latency problem conducted through the following steps. Firstly in Cross-validation, the data was split for train and test data. Secondly, the GridSearchCV conducted to tune the hyperplane best parameters. Thirdly SVR was used to fit the train data with polynomial, RBF, and sigmoid Kernel. Finally, the R square score

calculated on the test data. Figure 3.5 shows an overview of the methodology used for this phase.

The potentiality of using SVR for solving the latency problem

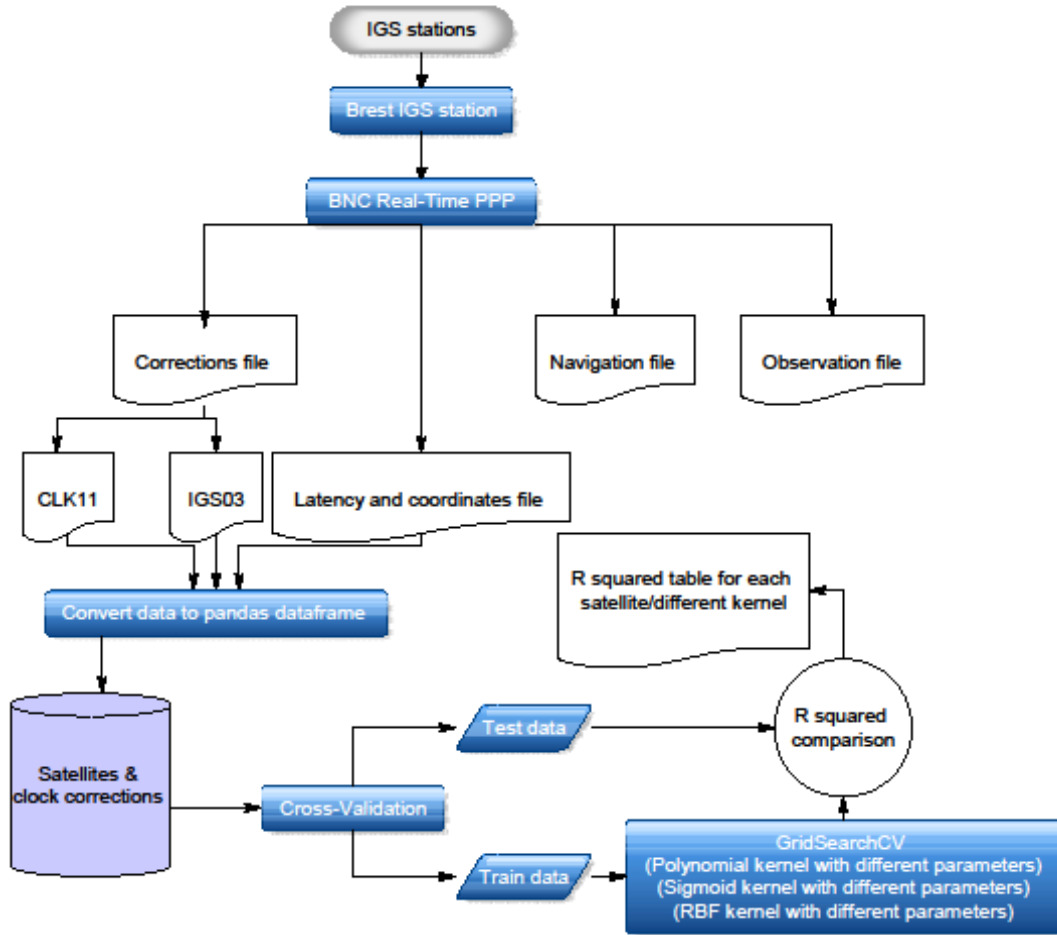


Figure 3-5 Potentiality of SVR in solving latency

3.4.2 Real-Time GNSS user simulation

In this phase, the BNC software was used in real-time PPP from around 9:26 o'clock on 13/12/2019 till 9:20 on 16/12/2019, the simulation for real-time scenarios is done by defining the concept of a sliding window. The data collected in the first minute used as ground truth and no prediction conducted on it. However, the new observation stored on the sliding window of data, as the old was dropped to maintain the same size. Meanwhile, the latency for the new observation is stored and used to define the offset span of prediction. Simultaneously the GridSearchCV conducted every 3.5 hours to define the best parameters in the case of the SVR. Consequently, the SVR and the RF used to predict the clock corrections according to the latency. Figure 3.6 shows the

illustration of real-time simulation. In this method, the GridSearchCV was not used to pick the best parameter of RF; thus, the RF was used with default parameters.

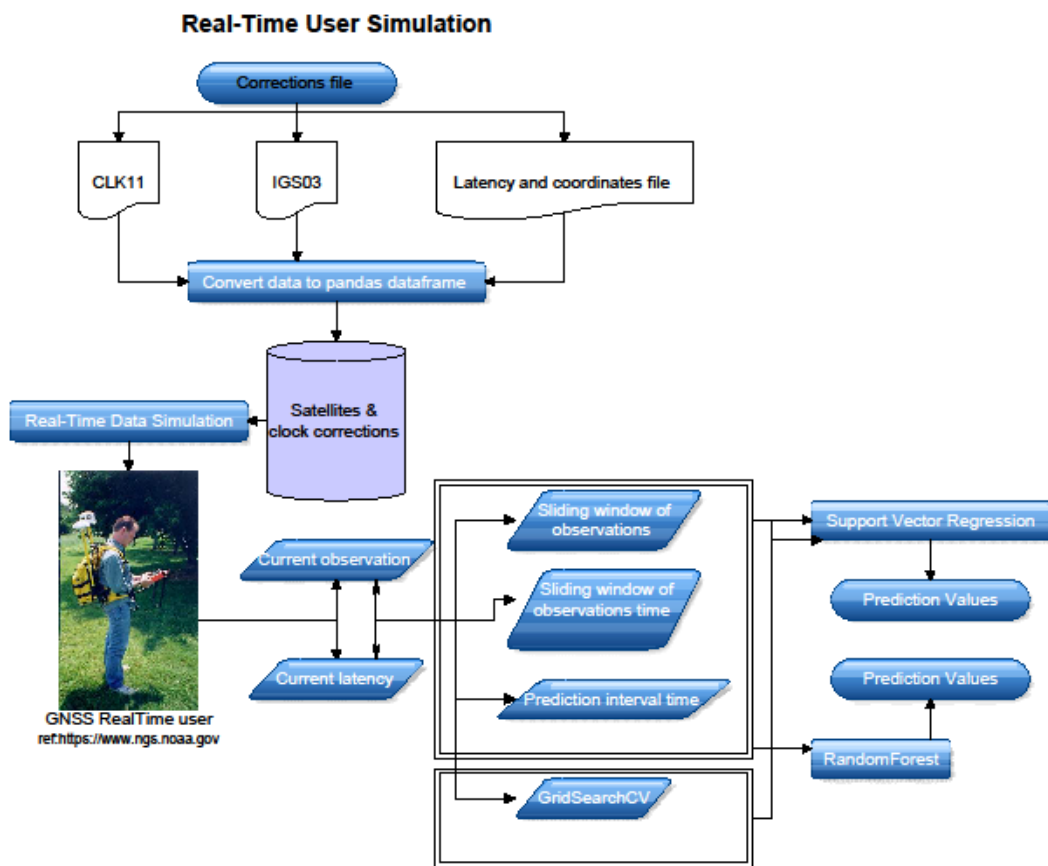


Figure 3-6 Real-time simulation

3.5 WP5 Visualization

In this work package, both Plotly, Matplotlib, and Seaborn visualization libraries are used to show both original values with prediction values obtained from both SVR and RF prediction models. Additionally, the histogram is used to show the distribution of the differences obtained among the original and prediction values. (Matplotlib, 2012; Plotly, 2018; Seaborn, 2012)

3.6 WP6 Statistical assessment

In fact, the correction file produced by the analysis center is not affected by latency. On the contrary, due to the processing and communication time, the GNSS user experienced around 10 seconds of latency in the CLK11 product and around 30 seconds latency in the IGS03 product. Thus, new datasets from the original data are

created with 10 and 30 seconds of simulated latency for CLK11 and IGS03, respectively. Then statistical assessment including range, mean, standard deviation, and R square value calculated on for the difference between the original values and latency shifted values. Consequently, the same statistical analysis was done for the differences of the values among the original and prediction values for both machine learning methods the SVR and the RF. Figure 3.7 shows the overview of steps performed in the statistical assessment phase.

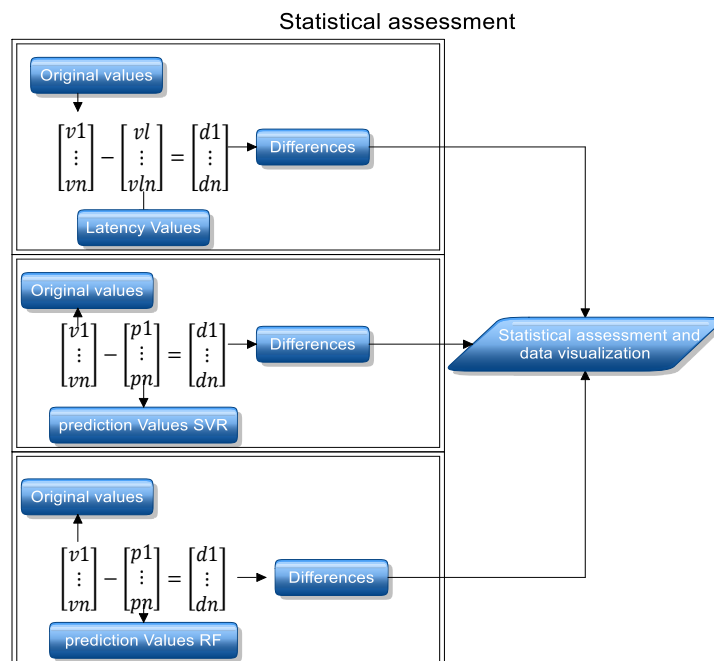


Figure 3-7 Statistical assessment of simulation phase

Chapter 4 Results and discussions

This chapter aims to provide the obtained results in this research. This chapter is divided into four main parts. The first part explains the latency values obtained from the BNC software. However, the second part explains the potentiality of applying SVR with different kernels for solving latency. Finally, the third part of this chapter focuses on the results obtained from the real-time simulation phase.

4.1 Latency values

The corrections provided with the IGS03 and the CLK11 products suffering from some latency values, which have slight fluctuations because of the processing and the internet speed. Table 4.1 shows the latency value in terms of mean, minimum, and maximum. BNC was recording the latency values during real-time PPP implementation for the IGS03 and the CLK11.

Table 4-1 IGS03 and CLK11 statistical summary of latency values

	IGS03 latency values	CLK11 latency values
Mean of latency values	31.68 seconds	7.51 seconds
Maximum of latency values	32.21 seconds	9.76 seconds
Minimum of latency values	31.34 seconds	6.20 seconds

4.2 Support vector regression parameter

The onboard satellite clocks act like data generators. The GNSS satellites disseminate signals stamps with transmission time generated individually by each satellite clock. However, the GNSS satellites have been launched with different blocks. Each block of satellites share more or less the same manufacturing components, signal structures, onboard clock, type of antenna,, etc. This research focuses on two GNSS systems the GPS and GLONASS. The current blocks on the GPS system are (IIF, III, IIR and, IIRM), while the GLONASS system contains M and K blocks.

Consequently, different types of clocks are implemented in each block with different characteristics in terms of frequency stability and frequency drift. Cesium and Rubidium deployed onboard GNSS satellites. More information about the types of clocks deployed in GLONASS and GPS can be found in (Cernigliaro, Valloreaia, Galleani, & Tavella, 2013; P. Daly, 1990; U.S.Department of Homeland security, 2020).

As mentioned, C and gamma values play a major role in the SVR model. Thus, the GridSearchCV method implemented to opt the best C and gamma combination. Figures 2.12 and 2.13 show the effect of those values in the SVR model. The following table shows the C and gamma values used to define the search parameters.

Table 4-2 C and gamma values

C values	0.1	1	10	100	1000
Gamma values	1	0.1	0.01	0.001	0.0001

Figures 4.1 and 4.2 show the effect of C and gamma values on the behavior of the SVR model. The following figures are obtained from data collected for around one day, between midnight on the 23rd of October, till midday on the 24th of October. The upper part of the figures shows the original values with respect to the prediction ones. While the lower part shows the difference in meters between the prediction and original values.

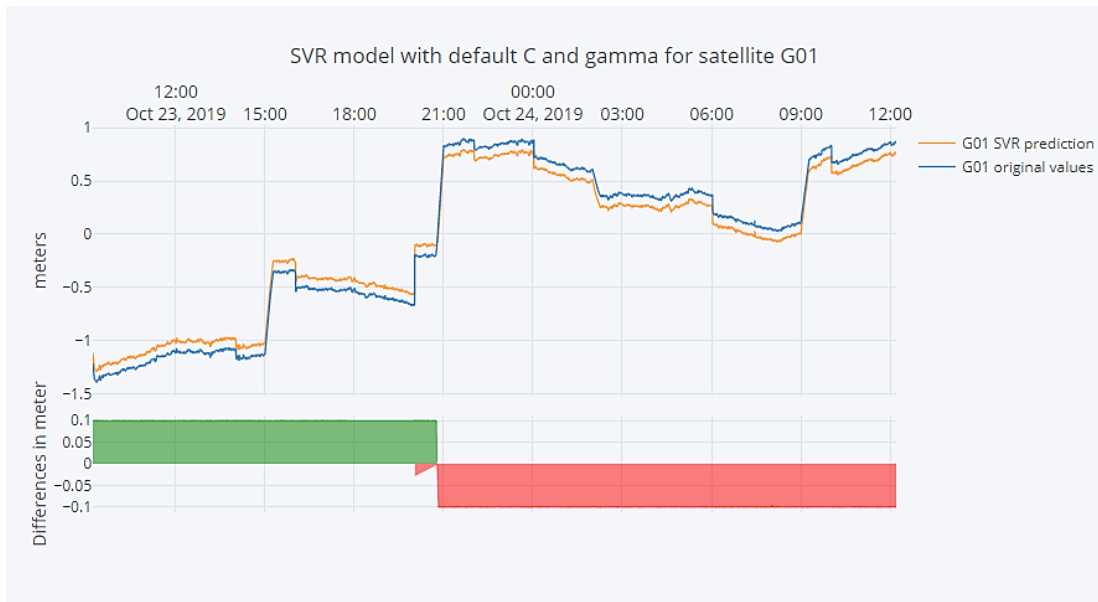


Figure 4-1 SVR with default parameters

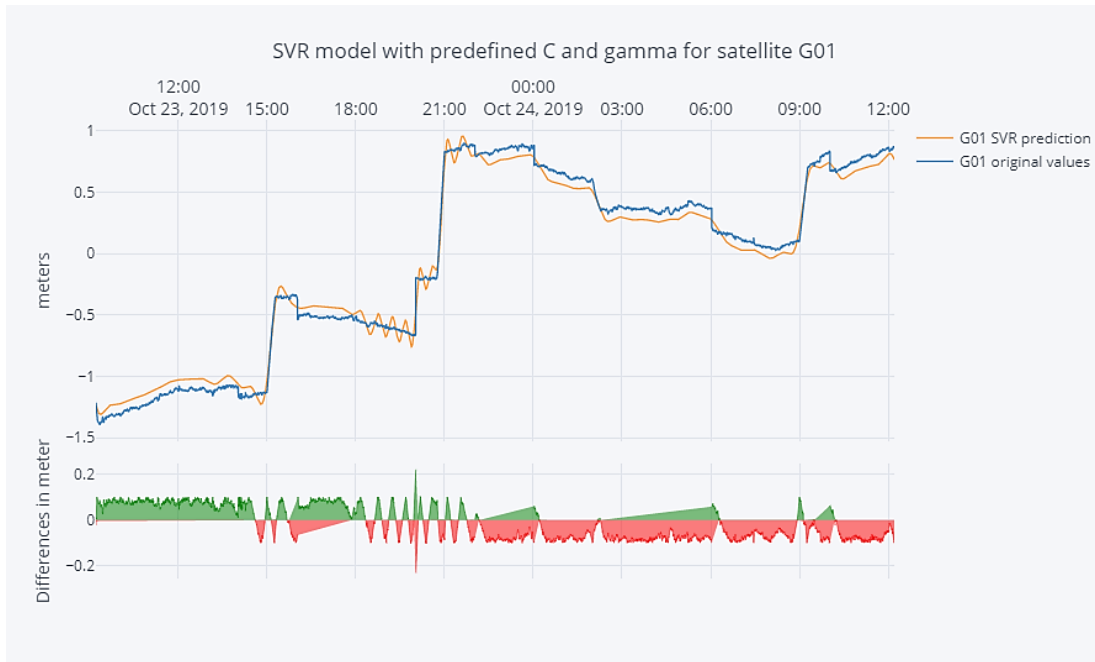


Figure 4-2 SVR with predefined parameters

The same dataset, which is used in the figures above, was divided into train and test datasets; through the cross-validation phase, the GridSearchCV implemented to pick the best gamma and C value combination for all satellites. Tables 4.3 and 4.4 show the best combination of C and gamma for all satellites in both the CLK11 and IGS03 correction files. The data on the following tables are grouped by different satellites block for both GLONASS and GPS systems.

Table 4-3 results of C and gamma for the IGS03 corrections

Satellites and Blocks	C	Gamma
IIF(G01,G03,G08,G24)	1000	0.001
IIF(G01,G03,G08,G24)	1000	0.0001
IIF(G06,G09,G11,G26,G27,G30,G32)	1	0.0001
IIR(G02,G11,G13,G16,G19,G21,G22,G23)	1	0.0001
IIR(G14,G28)	10	0.0001
IIR(G20)	100	0.0001
IIRM(G07,G12,G15)	1	0.0001
IIRM(G05,G29)	10	0.0001
IIRM(G17)	100	0.0001
IIRM(G31)	1000	0.0001
IIF(G320)	10	0.0001

Table 4-4 results of C and gamma for the CLK11 corrections

Satellites and Blocks	C	Gamma
IIF(G01,G03,G08,G24,G30)	1000	0.0001
IIF(G09,G10,G25)	10	0.0001
IIF(G06,G10,G26,G27)	1	0.0001
III(G04)	1	0.1
IIR(G13,G14)	1000	0.0001
IIR(G02,G11,G20,G23)	1	0.0001
IIR(G16,G19,G21,G22)	10	0.0001
IIRM(G05)	1	0.0001
IIRM(G12,G29)	100	0.0001
IIRM(G07,G15)	10	0.0001
IIRM(G17,G31)	1000	0.0001
K(R09)	100	0.0001
M(R01,R02,R08,R16,R18,R19,R20,R21,R23)	100	0.0001
M(R03)	10	0.01
M(R05,R12,R13,R14,R15,R17,R22,R24)	1000	0.0001
M(R07)	100	0.01

4.3 Support vector regression R² score and different kernel

The Scikit-Learn library implements the SVR with a different type of kernels. Thus, the methodology chapter in [section 3.4](#) investigated different types of kernels. 4th and 6th order polynomial, sigmoid, and Radial Base Function kernels. Consequently, the R² score is calculated to provide a sign of the quality of fitting; equation 4.1 shows the mathematical formula of the R² score.

$$R^2(y, \hat{y}) = 1 - \frac{\sum_{i=1}^n (y_i - \hat{y}_i)^2}{\sum_{i=1}^n (y_i - \bar{y})^2} \quad 4.1$$

The equation 4.1 can result in infinite values varies between 1 and -1. However, as much as a result comes closer to 1. That indicates that the developed model performs well (SciKit-Learn, 2016). The following tables show the R² score values obtained for both the IGS03 and CLK11; represent the performance R² score for each block of satellites.

Table 4-5 R² score values for different kernels IGS03

GPS block	Sigmoid	4th polynomial	6th order polynomial	RBF
IIF	-0.0143	0.6287	0.7143	0.7457
IIR	-0.0072	0.5679	0.6867	0.8759
IIRM	-0.0047	0.4276	0.6278	0.8849

Table 4-6 R² score values for different kernels CLK11

GNSS block	Sigmoid	4th polynomial	6 th order polynomial	RBF
IIF	-0.130490	0.871593	0.894979	0.986946
III	-0.430304	-0.128156	-0.127727	-0.430304
IIR	-0.124568	0.895931	0.917406	0.991701
IIRM	-0.164269	0.898718	0.917707	0.993447
K	-0.129862	0.866212	0.873549	0.991689
M	-0.094499	0.749322	0.813649	0.990985

4.4 Support vector regression and RandomForest in real-time simulation

The one-minute sliding window is implemented in a real-time scenario for both the IGS03 and CLK11. Due to the difference in sampling intervals, the IGS03 sliding window contains six entities, whereas the CLK11 sliding window contains twelve entities. After one minute of data storing, the SVR and the RF predict real-time observation according to the stored latency value stored by the real-time GNSS user. As mentioned before, the real-time user will use in the first minute the same correction values, where those values suffer from some latency, and no prediction conducted in the first minute.

Consequently, the statistical assessment with terms of mean, standard deviation, range, and R² score is conducted to investigate the performance for both SVR and RF. On one hand, the investigations were done by calculating the differences between the original and the prediction values. On the other hand, by calculating the differences between the original and latency values.

The following figures show the latency effect on both IGS03 and CLK11 products. The upper part of the figures shows the effect on the whole time-span of the dataset. While the lower part is the zoom cover around the first 40 minutes to show the latency effects in a closer zoom.

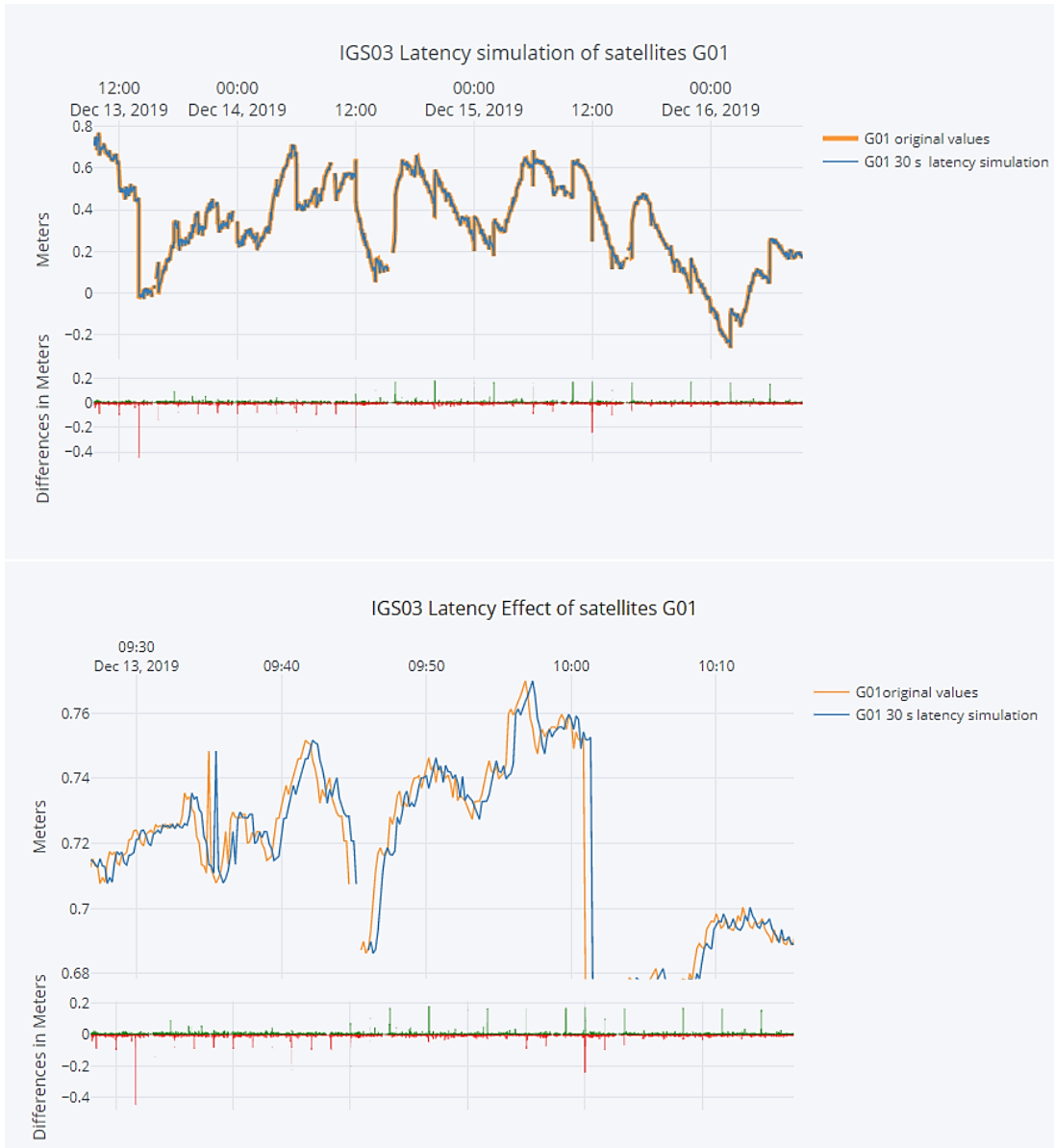


Figure 4-3 IGS03 30 seconds of latency effect on the satellite G01

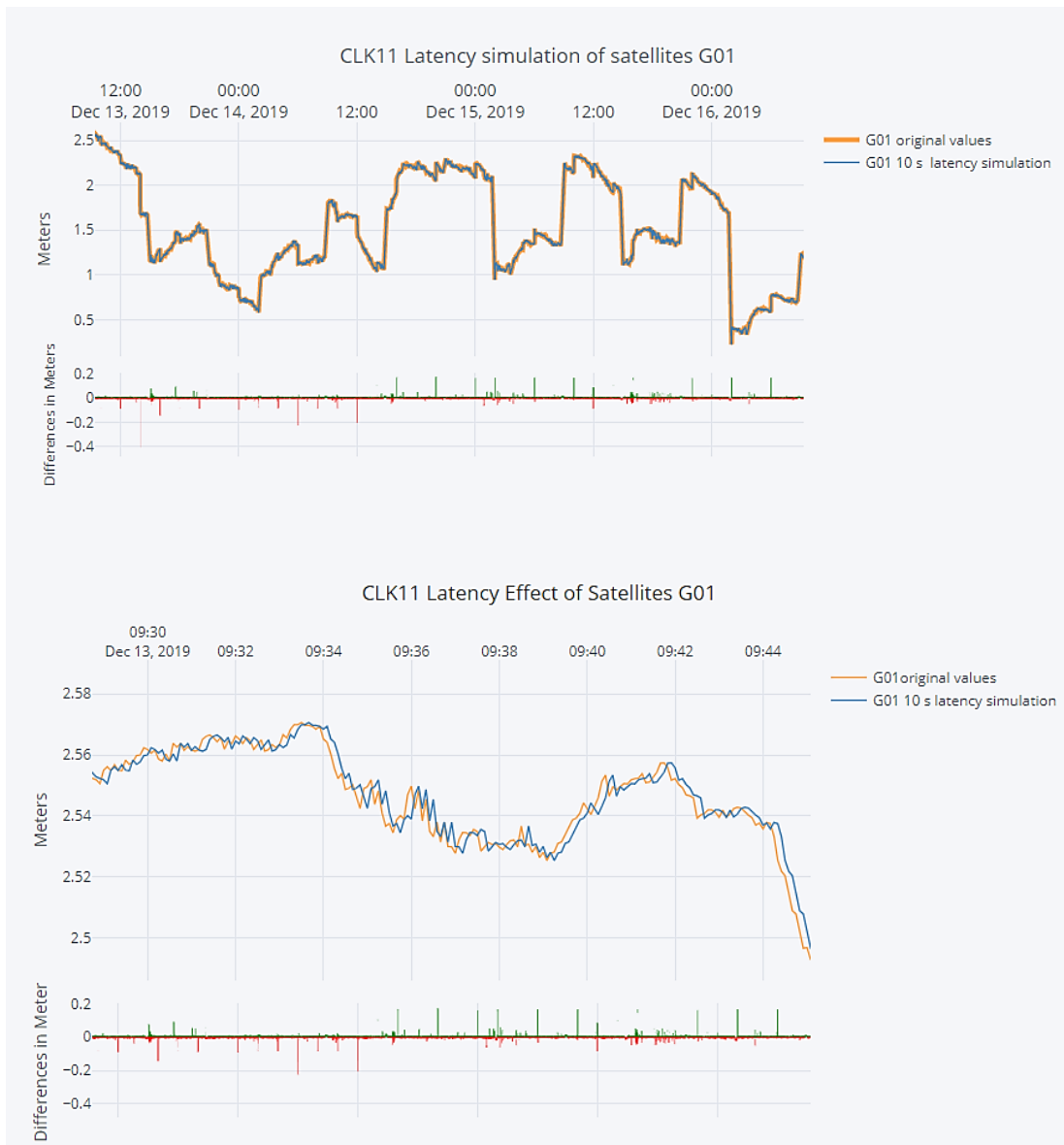


Figure 4-4 CLK11 10 seconds of latency effect on the satellite G01

The following tables show the statistical assessment of IGS03 corrections using the SVR method.

Table 4-7 IGS03 SVR statistical assessment for GPS satellites

Satellite #	Mean(m)		Standard deviation(m)		R ² Score		Range(m)		Satellite Block
	Latency	SVR	Latency	SVR	Latency	SVR	Latency	SVR	
G01	-0.0001	0.0000	0.0113	0.0070	0.9972	0.9989	0.6205	0.3274	IIF
G02	0.0000	0.0000	0.0224	0.0153	0.9880	0.9943	0.8641	0.4744	IIR
G03	0.0000	0.0000	0.0103	0.0067	0.9936	0.9973	0.6067	0.3538	IIF
G05	0.0000	0.0001	0.0330	0.0229	0.9748	0.9878	0.7442	0.4118	IIRM
G06	-0.0001	0.0001	0.0143	0.0090	0.9988	0.9995	1.1732	0.7420	IIF
G07	0.0001	-0.0001	0.0248	0.0169	0.9959	0.9981	0.8709	0.4885	IIRM
G08	0.0000	-0.0001	0.0338	0.0229	0.9976	0.9989	2.2258	1.7026	IIF
G09	0.0000	-0.0001	0.0103	0.0086	0.9963	0.9974	0.7048	1.1413	IIF
G10	0.0001	-0.0001	0.0089	0.0059	0.9985	0.9993	0.4918	0.2681	IIF
G11	0.0000	-0.0003	0.0246	0.0321	0.9969	0.9947	1.3221	4.3078	IIR
G12	0.0000	0.0000	0.0285	0.0196	0.9788	0.9899	0.4325	0.2523	IIRM
G13	-0.0001	0.0001	0.0206	0.0142	0.9854	0.9930	0.4720	0.2844	IIR
G14	-0.0001	0.0000	0.0209	0.0146	0.9897	0.9950	0.3849	0.2190	IIR
G15	0.0000	0.0000	0.0227	0.0156	0.9894	0.9950	0.9703	0.5850	IIRM
G16	0.0000	0.0000	0.0270	0.0187	0.9895	0.9950	0.7205	0.4266	IIR
G17	0.0001	-0.0002	0.0335	0.0599	0.9963	0.9882	2.4437	12.2479	IIRM
G19	0.0000	0.0000	0.0227	0.0159	0.9889	0.9945	0.3508	0.1840	IIR
G20	0.0000	0.0000	0.0240	0.0167	0.9728	0.9866	0.7112	0.4809	IIR
G21	0.0000	-0.0001	0.0325	0.0225	0.9805	0.9906	1.0143	0.6841	IIR
G22	0.0000	0.0000	0.0230	0.0162	0.9809	0.9904	0.3534	0.2069	IIR
G23	0.0000	0.0000	0.0218	0.0147	0.9871	0.9941	1.0757	0.5593	IIR
G24	0.0003	0.0000	0.0597	0.1863	0.9979	0.9798	5.3156	35.6869	IIF
G25	-0.0001	0.0000	0.0102	0.0064	0.9975	0.9990	0.7411	0.4512	IIF
G26	0.0000	0.0000	0.0086	0.0058	0.9974	0.9989	0.3563	0.1809	IIF
G27	0.0000	0.0000	0.0102	0.0065	0.9976	0.9990	0.7045	0.4642	IIF
G28	0.0000	0.0001	0.0393	0.0906	0.9978	0.9886	3.7002	17.5401	IIR
G29	-0.0001	0.0000	0.0276	0.0187	0.9924	0.9965	1.5745	1.1266	IIRM
G30	0.0000	0.0000	0.0119	0.0075	0.9981	0.9992	0.9810	0.6016	IIF
G31	0.0000	0.0000	0.0248	0.0195	0.9881	0.9927	1.4787	2.2783	IIRM
G32	0.0000	0.0000	0.0107	0.0069	0.9964	0.9985	0.7018	0.4114	IIF

Table 4-8 IGS03 SVR statistical assessment for GLONASS satellites

Satellite #	Mean(m)		Standard deviation(m)		R ² Score		Range(m)		Satellite Block
	Latency	SVR	Latency	SVR	Latency	SVR	Latency	SVR	
R01	-0.0001	-0.0023	0.0484	0.0419	0.9867	0.9902	1.1643	4.4143	M
R02	0.0000	-0.0007	0.0551	0.1015	0.9982	0.9938	3.7414	18.6735	M
R03	0.0000	-0.0005	0.0395	0.0501	0.9968	0.9950	1.8283	9.2806	M
R05	0.0000	0.0000	0.0370	0.0579	0.9946	0.9870	2.5240	10.5458	M
R07	-0.0001	0.0022	0.0444	0.0490	0.9937	0.9923	1.6680	5.4284	M
R08	0.0002	0.0007	0.0684	0.1528	0.9989	0.9943	5.9380	31.1214	M
R09	0.0001	-0.0002	0.0373	0.0514	0.9976	0.9955	2.8167	7.5229	K
R11	-0.0003	0.0009	0.0424	0.0281	0.9973	0.9988	1.5080	1.4093	M
R12	0.0003	0.0005	0.0355	0.0566	0.9983	0.9956	2.5162	9.1016	M
R13	0.0004	0.0004	0.0643	0.0487	0.9970	0.9986	3.9650	4.4662	M
R14	-0.0001	-0.0006	0.0400	0.0258	0.9939	0.9974	1.4249	1.2633	M
R15	-0.0001	-0.0003	0.0283	0.0177	0.9965	0.9987	1.1495	0.6464	M
R16	-0.0001	-0.0007	0.0480	0.0850	0.9981	0.9941	2.8507	12.7612	M
R17	0.0000	-0.0012	0.0422	0.0328	0.9840	0.9903	1.1271	1.8113	M
R18	0.0003	-0.0012	0.0510	0.0358	0.9984	0.9992	2.8527	2.3408	M
R19	0.0002	0.0006	0.0399	0.0338	0.9944	0.9960	1.1674	2.8863	M
R20	-0.0002	0.0020	0.0472	0.0667	0.9909	0.9820	1.9188	12.5743	M
R21	0.0000	-0.0002	0.0330	0.0536	0.9981	0.9950	2.2598	10.9902	M
R22	-0.0003	0.0012	0.0558	0.0725	0.9987	0.9978	3.9306	12.6076	M
R23	0.0002	-0.0022	0.0511	0.0408	0.9959	0.9974	1.1816	2.0152	M

The SVR method developed some outliers. Thus, the threshold was constructed to detect them; consequently, whenever the prediction value had a 2-meter magnitude or more, real-time GNSS users will use the current observation value instead of the predicted one. Tables 4.9 and 4.10 are a repetition of tables 4.7 and 4.8 after resolving the outliers.

Table 4-9 IGS03 SVR statistical assessment for GPS satellites

Satellite #	Mean(m)		Standard deviation(m)		R ² Score		Range(m)		Satellite Block
	Latency	SVR	Latency	SVR	Latency	SVR	Latency	SVR	
G01	-0.0001	0.0000	0.0113	0.0070	0.9972	0.9989	0.6205	0.3274	IIF
G02	0.0000	0.0000	0.0224	0.0153	0.9880	0.9943	0.8641	0.4744	IIR
G03	0.0000	0.0000	0.0103	0.0067	0.9936	0.9973	0.6067	0.3538	IIF
G05	0.0000	0.0001	0.0330	0.0229	0.9748	0.9878	0.7442	0.4118	IIRM
G06	-0.0001	0.0001	0.0143	0.0090	0.9988	0.9995	1.1732	0.7420	IIF
G07	0.0001	-0.0001	0.0248	0.0169	0.9959	0.9981	0.8709	0.4885	IIRM
G08	0.0000	-0.0001	0.0338	0.0229	0.9976	0.9989	2.2258	1.7026	IIF
G09	0.0000	0.0000	0.0103	0.0098	0.9963	0.9966	0.7048	1.3036	IIF
G10	0.0001	-0.0001	0.0089	0.0059	0.9985	0.9993	0.4918	0.2681	IIF
G11	0.0000	0.0000	0.0246	0.0188	0.9969	0.9982	1.3221	1.7365	IIR
G12	0.0000	0.0000	0.0285	0.0196	0.9788	0.9899	0.4325	0.2523	IIRM
G13	-0.0001	0.0001	0.0206	0.0142	0.9854	0.9930	0.4720	0.2844	IIR
G14	-0.0001	0.0000	0.0209	0.0146	0.9897	0.9950	0.3849	0.2190	IIR
G15	0.0000	0.0000	0.0227	0.0156	0.9894	0.9950	0.9703	0.5850	IIRM
G16	0.0000	0.0000	0.0270	0.0187	0.9895	0.9950	0.7205	0.4266	IIR
G17	0.0001	-0.0002	0.0335	0.0233	0.9963	0.9982	2.4437	2.0780	IIRM
G19	0.0000	0.0000	0.0227	0.0159	0.9889	0.9945	0.3508	0.1840	IIR
G20	0.0000	0.0000	0.0240	0.0167	0.9728	0.9866	0.7112	0.4809	IIR
G21	0.0000	-0.0001	0.0325	0.0225	0.9805	0.9906	1.0143	0.6841	IIR
G22	0.0000	0.0000	0.0230	0.0162	0.9809	0.9904	0.3534	0.2069	IIR
G23	0.0000	0.0000	0.0218	0.0147	0.9871	0.9941	1.0757	0.5593	IIR
G24	0.0003	-0.0001	0.0597	0.0401	0.9979	0.9990	5.3156	5.2552	IIF
G25	-0.0001	0.0000	0.0102	0.0064	0.9975	0.9990	0.7411	0.4512	IIF
G26	0.0000	0.0000	0.0086	0.0058	0.9974	0.9989	0.3563	0.1809	IIF
G27	0.0000	0.0000	0.0102	0.0065	0.9976	0.9990	0.7045	0.4642	IIF
G28	0.0000	0.0003	0.0393	0.0255	0.9978	0.9991	3.7002	2.7079	IIR
G29	-0.0001	0.0000	0.0276	0.0187	0.9924	0.9965	1.5745	1.1266	IIRM
G30	0.0000	0.0000	0.0119	0.0075	0.9981	0.9992	0.9810	0.6016	IIF
G31	0.0000	0.0000	0.0248	0.0207	0.9881	0.9918	1.4787	2.2649	IIRM
G32	0.0000	0.0000	0.0107	0.0069	0.9964	0.9985	0.7018	0.4114	IIF

Table 4-10 IGS03 SVR statistical assessment for GLONASS satellites

Satellite #	Mean(m)		Standard deviation(m)		R ² Score		Range(m)		Satellite Block
	Latency	SVR	Latency	SVR	Latency	SVR	Latency	SVR	
R01	-0.0001	-0.0016	0.0484	0.0403	0.9867	0.9909	1.1643	3.3201	M
R02	0.0000	-0.0002	0.0551	0.0392	0.9982	0.9991	3.7414	3.0990	M
R03	0.0000	-0.0003	0.0395	0.0312	0.9968	0.9980	1.8283	2.8267	M
R05	0.0000	-0.0001	0.0370	0.0251	0.9946	0.9975	2.5240	2.7477	M
R07	-0.0001	0.0008	0.0444	0.0330	0.9937	0.9965	1.6680	2.0547	M
R08	0.0002	0.0000	0.0684	0.0521	0.9989	0.9993	5.9380	5.8922	M
R09	0.0001	0.0001	0.0373	0.0258	0.9976	0.9989	2.8167	2.1808	K
R11	-0.0003	0.0009	0.0424	0.0281	0.9973	0.9988	1.5080	1.4093	M
R12	0.0003	0.0003	0.0355	0.0268	0.9983	0.9990	2.5162	3.3305	M
R13	0.0004	0.0011	0.0643	0.0468	0.9970	0.9987	3.9650	4.9324	M
R14	-0.0001	-0.0006	0.0400	0.0258	0.9939	0.9974	1.4249	1.2633	M
R15	-0.0001	-0.0003	0.0283	0.0177	0.9965	0.9987	1.1495	0.6464	M
R16	-0.0001	-0.0006	0.0480	0.0455	0.9981	0.9983	2.8507	3.6038	M
R17	0.0000	-0.0005	0.0422	0.0361	0.9840	0.9882	1.1271	2.0152	M
R18	0.0003	-0.0012	0.0510	0.0358	0.9984	0.9992	2.8527	2.3408	M
R19	0.0002	0.0001	0.0399	0.0316	0.9944	0.9965	1.1674	2.3588	M
R20	-0.0002	0.0013	0.0472	0.0375	0.9909	0.9942	1.9188	2.2181	M
R21	0.0000	-0.0003	0.0330	0.0236	0.9981	0.9990	2.2598	2.2978	M
R22	-0.0003	0.0005	0.0558	0.0459	0.9987	0.9991	3.9306	4.7456	M
R23	0.0002	-0.0015	0.0511	0.0451	0.9959	0.9968	1.1816	1.9870	M

The following tables show the statistical assessment of CLK11 corrections using the SVR method.

Table 4-11 CLK11 SVR statistical assessment for GPS satellites

Satellite #	Mean(m)		Standard deviation(m)		R ² Score		Range(m)		Satellite Block
	Latency	SVR	Latency	SVR	Latency	SVR	Latency	SVR	
G01	-0.0001	0.0001	0.0066	0.0087	0.9999	0.9998	0.6157	0.3018	IIF
G02	0.0000	0.0000	0.0105	0.0165	0.9996	0.9990	0.9073	0.4571	IIR
G03	0.0000	0.0000	0.0061	0.0082	0.9999	0.9997	0.6016	0.3532	IIF
G05	0.0000	0.0001	0.0150	0.0246	0.9993	0.9981	0.7136	0.4761	IIRM
G06	-0.0001	0.0001	0.0087	0.0091	0.9998	0.9998	1.4514	1.0874	IIF
G07	0.0000	0.0000	0.0118	0.0182	0.9997	0.9994	0.7864	0.4013	IIRM
G08	0.0000	-0.0001	0.0182	0.0238	0.9996	0.9993	2.2007	1.7567	IIF
G09	0.0000	0.0000	0.0062	0.0082	0.9999	0.9998	0.7078	0.2744	IIF
G10	0.0000	0.0000	0.0052	0.0077	0.9999	0.9998	0.4943	0.2530	IIF
G11	0.0000	0.0000	0.0117	0.0179	0.9998	0.9994	1.3365	0.6209	IIR
G12	0.0000	-0.0001	0.0128	0.0213	0.9996	0.9987	0.4893	0.2620	IIRM
G13	0.0000	0.0001	0.0100	0.0159	0.9997	0.9992	0.4367	0.2328	IIR
G14	0.0000	0.0001	0.0098	0.0164	0.9997	0.9992	0.4811	0.2421	IIR
G15	0.0000	0.0000	0.0109	0.0174	0.9995	0.9986	0.9718	0.7666	IIRM
G16	0.0000	0.0000	0.0122	0.0203	0.9997	0.9991	0.6185	0.1994	IIR
G17	0.0000	-0.0001	0.0166	0.0216	0.9991	0.9985	2.4014	0.9427	IIRM
G19	0.0000	0.0001	0.0104	0.0177	0.9997	0.9991	0.3356	0.1945	IIR
G20	0.0000	0.0000	0.0110	0.0188	0.9996	0.9987	0.7361	0.5390	IIR
G21	0.0000	-0.0001	0.0147	0.0237	0.9991	0.9977	1.1309	0.4174	IIR
G22	0.0000	0.0001	0.0103	0.0180	0.9997	0.9991	0.3049	0.1931	IIR
G23	0.0000	0.0001	0.0104	0.0160	0.9996	0.9992	1.0675	0.2619	IIR
G24	0.0001	-0.0001	0.0332	0.0470	0.9993	0.9986	5.2809	8.4630	IIF
G25	0.0000	0.0001	0.0060	0.0079	0.9999	0.9998	0.6938	0.3696	IIF
G26	-0.0001	0.0001	0.0051	0.0080	0.9999	0.9998	0.3571	0.4239	IIF
G27	0.0000	0.0001	0.0061	0.0083	0.9999	0.9998	0.7030	0.5045	IIF
G28	0.0000	0.0002	0.0208	0.0177	0.9997	0.9998	3.8039	0.4870	IIR
G29	0.0000	0.0001	0.0135	0.0187	0.9991	0.9982	1.5520	0.8010	IIRM
G30	0.0000	0.0000	0.0070	0.0085	0.9998	0.9997	0.9766	0.5250	IIF
G31	0.0000	0.0000	0.0122	0.0188	0.9996	0.9990	1.5132	1.3180	IIRM
G32	0.0000	0.0000	0.0063	0.0081	0.9999	0.9998	0.7064	0.2903	IIF

Table 4-12 CLK11 SVR statistical assessment for GLONASS satellites

Satellite #	Mean(m)		Standard deviation(m)		R ² Score		Range(m)		Satellite Block
	Latency	SVR	Latency	SVR	Latency	SVR	Latency	SVR	
R01	0.0000	-0.0019	0.0281	0.0263	0.9983	0.9985	1.1437	1.3172	M
R02	0.0000	-0.0009	0.0328	0.0380	0.9996	0.9994	3.6820	3.4736	M
R03	0.0000	-0.0007	0.0225	0.0262	0.9993	0.9994	1.7044	2.6058	M
R05	0.0000	0.0002	0.0215	0.0232	0.9990	0.9988	2.5159	2.1690	M
R07	0.0000	0.0012	0.0263	0.0243	0.9991	0.9993	1.6672	0.8312	M
R08	0.0001	0.0010	0.0397	0.0452	0.9994	0.9993	5.9137	5.7046	M
R09	0.0000	0.0001	0.0210	0.0266	0.9995	0.9993	2.8091	2.2349	K
R11	-0.0001	0.0013	0.0267	0.0257	0.9997	0.9997	3.5225	1.9625	M
R12	0.0001	0.0000	0.0202	0.0198	0.9995	0.9995	2.5288	1.3204	M
R13	0.0001	0.0023	0.0379	0.0378	0.9995	0.9995	4.8305	2.3716	M
R14	0.0000	-0.0013	0.0230	0.0217	0.9995	0.9996	1.4032	1.3037	M
R15	0.0000	-0.0003	0.0162	0.0173	0.9998	0.9997	1.1296	0.7181	M
R16	0.0001	-0.0006	0.0279	0.0306	0.9995	0.9994	2.8219	2.9444	M
R17	0.0000	-0.0012	0.0243	0.0216	0.9987	0.9990	1.1255	0.7575	M
R18	0.0001	-0.0016	0.0297	0.0239	0.9996	0.9998	2.8272	1.0490	M
R19	0.0001	0.0008	0.0234	0.0221	0.9991	0.9992	1.1371	1.2331	M
R20	-0.0001	0.0012	0.0275	0.0305	0.9987	0.9984	1.9539	1.7621	M
R21	0.0000	-0.0003	0.0189	0.0196	0.9991	0.9990	2.2431	1.5262	M
R22	-0.0001	0.0013	0.0323	0.0379	0.9996	0.9994	3.9373	8.9434	M
R23	0.0001	-0.0025	0.0299	0.0303	0.9990	0.9991	1.1330	1.6672	M

In the following figures, the SVR model with respect to the original data, as well as the histogram, are used to show the distribution of the differences for both IGS03 and CLK11 corrections files. The GPS satellite PRN G01 is picked as representer of all the datasets of satellites.

The upper part of the figure shows the SVR model with original values for satellite G01, with respect to the prediction values obtained with SVR for the IGS03 correction file, while the lower part shows the difference in meter between original and prediction values.

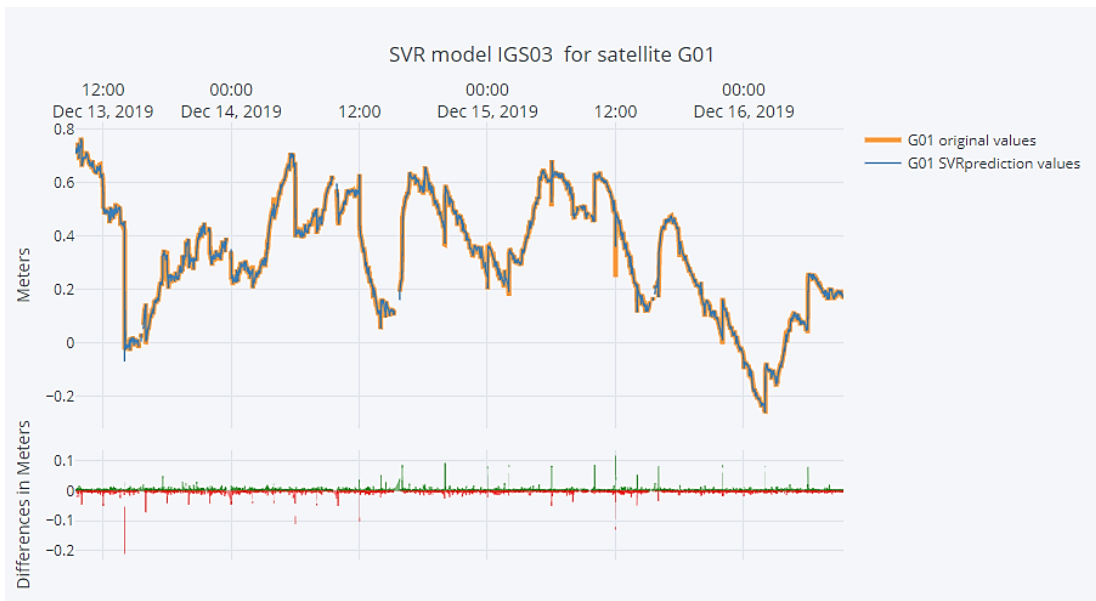


Figure 4-5 IGS03 SVR model for satellite G01

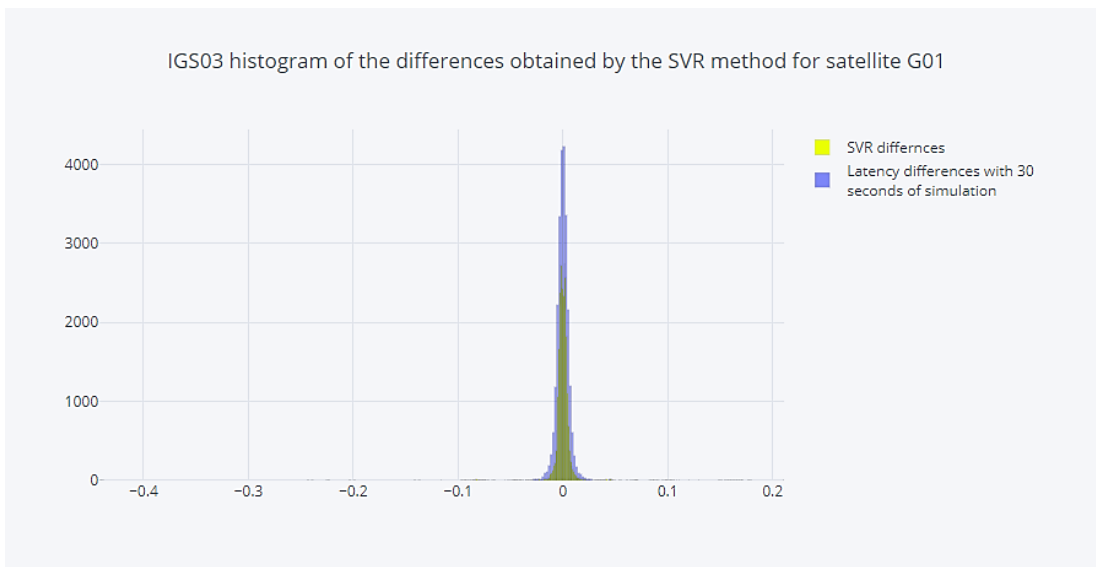


Figure 4-6 IGS03 histogram of the differences obtained by the SVR method for satellite G01

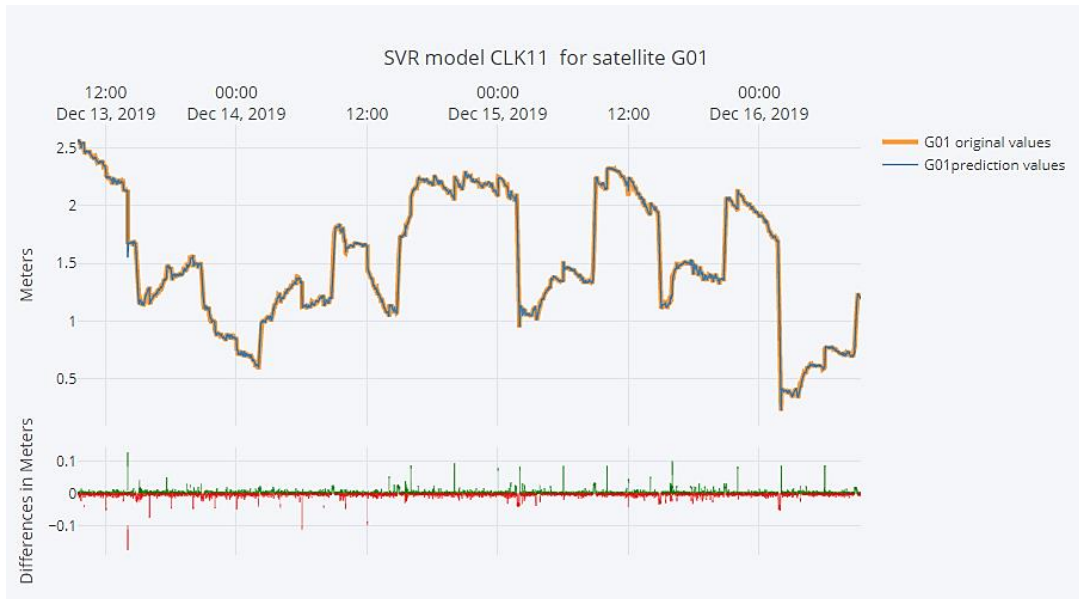


Figure 4-7 CLK11 SVR model for satellite G01

The upper part of Figure 4-7 shows the SVR model with original values for satellite G01, with respect to the prediction values obtained with SVR for the CLK11 correction file, while the lower part shows the difference in meter between original and prediction values.

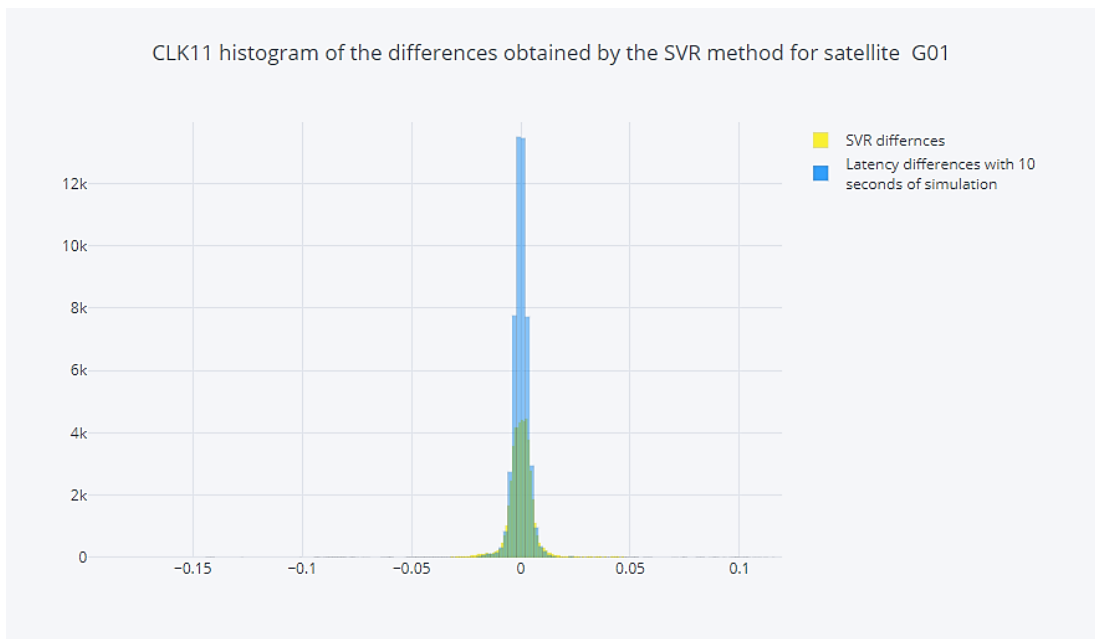


Figure 4-8 CLK11 histogram of the differences obtained by the SVR method for satellite G01

The following tables show the statistical assessment of IGS03 and CLK11 corrections using the RF method. The following figures show the RF model with respect to the original data, as well as the histogram, which are used to show the distribution of the differences for both IGS03 and CLK11 corrections files.

Table 4-13 IGS03 RF statistical assessment for GPS satellites

Satellite #	Mean(m)		Standard deviation(m)		R ² Score		Range(m)		Satellite Block
	Latency	RF	Latency	RF	Latency	RF	Latency	RF	
G01	-0.0001	0.0000	0.0113	0.0023	0.9972	0.9999	0.6205	0.1568	IIF
G02	0.0000	0.0000	0.0224	0.0040	0.9880	0.9996	0.8641	0.1726	IIR
G03	0.0000	0.0000	0.0103	0.0019	0.9936	0.9998	0.6067	0.1429	IIF
G05	0.0000	0.0000	0.0330	0.0060	0.9748	0.9992	0.7442	0.1438	IIRM
G06	-0.0001	0.0000	0.0143	0.0024	0.9988	1.0000	1.1732	0.2552	IIF
G07	0.0001	0.0000	0.0248	0.0043	0.9959	0.9999	0.8709	0.1499	IIRM
G08	0.0000	0.0000	0.0338	0.0061	0.9976	0.9999	2.2258	0.4474	IIF
G09	0.0000	0.0000	0.0103	0.0020	0.9963	0.9999	0.7048	0.1403	IIF
G10	0.0001	0.0000	0.0089	0.0018	0.9985	0.9999	0.4918	0.1357	IIF
G11	0.0000	0.0000	0.0246	0.0041	0.9969	0.9999	1.3221	0.2760	IIR
G12	0.0000	0.0000	0.0285	0.0051	0.9788	0.9993	0.4325	0.1434	IIRM
G13	-0.0001	0.0000	0.0206	0.0039	0.9854	0.9995	0.4720	0.1198	IIR
G14	-0.0001	0.0000	0.0209	0.0039	0.9897	0.9997	0.3849	0.1149	IIR
G15	0.0000	0.0000	0.0227	0.0041	0.9894	0.9997	0.9703	0.2063	IIRM
G16	0.0000	0.0000	0.0270	0.0048	0.9895	0.9997	0.7205	0.1439	IIR
G17	0.0001	0.0000	0.0335	0.0054	0.9963	0.9999	2.4437	0.4808	IIRM
G19	0.0000	0.0000	0.0227	0.0042	0.9889	0.9996	0.3508	0.1303	IIR
G20	0.0000	0.0000	0.0240	0.0043	0.9728	0.9991	0.7112	0.1756	IIR
G21	0.0000	0.0000	0.0325	0.0057	0.9805	0.9994	1.0143	0.2126	IIR
G22	0.0000	0.0000	0.0230	0.0041	0.9809	0.9994	0.3534	0.1194	IIR
G23	0.0000	0.0000	0.0218	0.0039	0.9871	0.9996	1.0757	0.2030	IIR
G24	0.0003	0.0000	0.0597	0.0098	0.9979	0.9999	5.3156	1.0483	IIF
G25	-0.0001	0.0000	0.0102	0.0018	0.9975	0.9999	0.7411	0.1366	IIF
G26	0.0000	0.0000	0.0086	0.0018	0.9974	0.9999	0.3563	0.0945	IIF
G27	0.0000	0.0000	0.0102	0.0019	0.9976	0.9999	0.7045	0.1404	IIF
G28	0.0000	0.0000	0.0393	0.0063	0.9978	0.9999	3.7002	0.8969	IIR
G29	-0.0001	0.0000	0.0276	0.0047	0.9924	0.9998	1.5745	0.3114	IIRM
G30	0.0000	0.0000	0.0119	0.0022	0.9981	0.9999	0.9810	0.2251	IIF
G31	0.0000	0.0000	0.0248	0.0043	0.9881	0.9996	1.4787	0.2883	IIRM
G32	0.0000	0.0000	0.0107	0.0020	0.9964	0.9999	0.7018	0.1797	IIF

Table 4-14 IGS03 RF statistical assessment for GLONASS satellites

Satellite #	Mean(m)		Standard deviation(m)		R ² Score		Range(m)		Satellite Block
	Latency	RF	Latency	RF	Latency	RF	Latency	RF	
R01	-0.0001	-0.0003	0.0484	0.0073	0.9867	0.9997	1.1643	0.2409	M
R02	0.0000	-0.0002	0.0551	0.0096	0.9982	0.9999	3.7414	0.7376	M
R03	0.0000	-0.0001	0.0395	0.0062	0.9968	0.9999	1.8283	0.3625	M
R05	0.0000	0.0001	0.0370	0.0063	0.9946	0.9998	2.5240	0.4985	M
R07	-0.0001	0.0002	0.0444	0.0071	0.9937	0.9998	1.6680	0.3289	M
R08	0.0002	0.0001	0.0684	0.0098	0.9989	1.0000	5.9380	1.1796	M
R09	0.0001	0.0000	0.0373	0.0067	0.9976	0.9999	2.8167	0.5587	K
R11	-0.0003	0.0002	0.0424	0.0065	0.9973	0.9999	1.5080	0.2974	M
R12	0.0003	0.0000	0.0355	0.0057	0.9983	1.0000	2.5162	0.5026	M
R13	0.0004	0.0002	0.0643	0.0114	0.9970	0.9999	3.9650	0.9997	M
R14	-0.0001	-0.0002	0.0400	0.0062	0.9939	0.9999	1.4249	0.3029	M
R15	-0.0001	0.0000	0.0283	0.0049	0.9965	0.9999	1.1495	0.2265	M
R16	-0.0001	0.0000	0.0480	0.0073	0.9981	1.0000	2.8507	0.5609	M
R17	0.0000	-0.0002	0.0422	0.0067	0.9840	0.9996	1.1271	0.2247	M
R18	0.0003	-0.0002	0.0510	0.0075	0.9984	1.0000	2.8527	0.5618	M
R19	0.0002	0.0001	0.0399	0.0070	0.9944	0.9998	1.1674	0.2637	M
R20	-0.0002	0.0002	0.0472	0.0075	0.9909	0.9998	1.9188	0.3814	M
R21	0.0000	0.0000	0.0330	0.0055	0.9981	0.9999	2.2598	0.4472	M
R22	-0.0003	0.0002	0.0558	0.0079	0.9987	1.0000	3.9306	0.7807	M
R23	0.0002	-0.0003	0.0511	0.0082	0.9959	0.9999	1.1816	0.2286	M

The upper part of Figure 4-9 shows the RF model with original values for satellite G01, with respect to the prediction values obtained with RF for the IGS03 correction file, while the lower part shows the difference in meter between original and prediction values. While Figure 4-10 is the histogram that shows the frequency and the distribution of the differences.

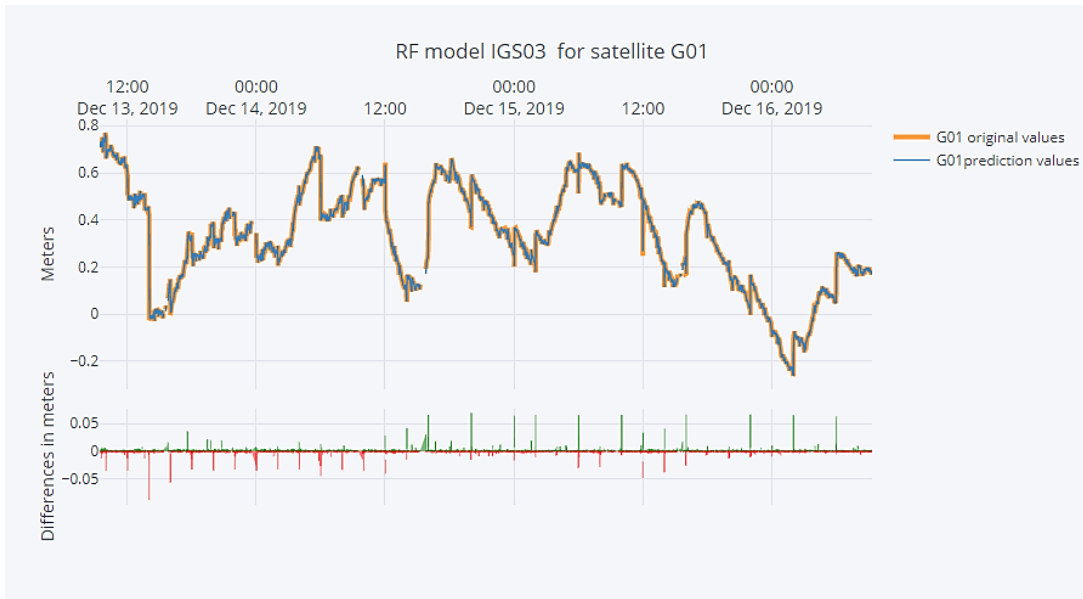


Figure 4-9 IGS03 RF model for satellite G01

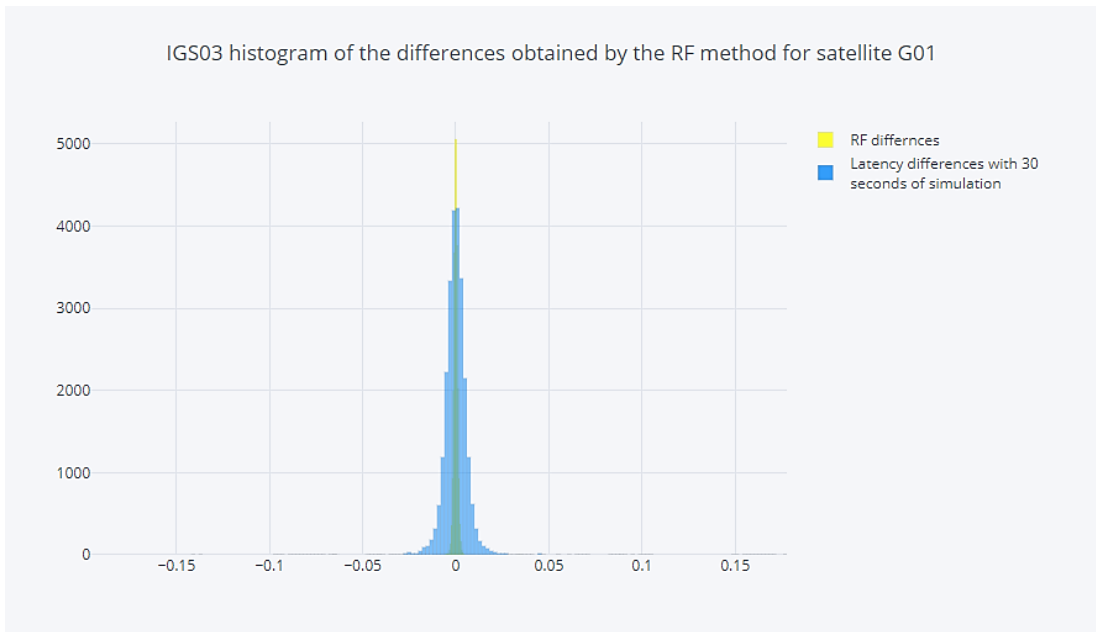


Figure 4-10 IGS03 histogram of the differences obtained by the RF method for satellite G01

The following tables show the statistical assessment of CLK11 corrections using the RF method.

Table 4-15 CLK11 RF statistical assessment for GPS satellites

Satellite #	Mean(m)		Standard deviation(m)		R ² Score		Range(m)		Satellite Block
	Latency	RF	Latency	RF	Latency	RF	Latency	RF	
G01	-0.0001	0.0000	0.0066	0.0013	0.9999	0.999995	0.6157	0.2112	IIF
G02	0.0000	0.0000	0.0105	0.0018	0.9996	0.999987	0.9073	0.3638	IIR
G03	0.0000	0.0000	0.0061	0.0013	0.9999	0.999993	0.6016	0.2104	IIF
G05	0.0000	0.0000	0.0150	0.0021	0.9993	0.999987	0.7136	0.2834	IIRM
G06	-0.0001	0.0000	0.0087	0.0022	0.9998	0.999989	1.4514	0.5805	IIF
G07	0.0000	0.0000	0.0118	0.0021	0.9997	0.999992	0.7864	0.2800	IIRM
G08	0.0000	0.0000	0.0182	0.0039	0.9996	0.999980	2.2007	0.8761	IIF
G09	0.0000	0.0000	0.0062	0.0013	0.9999	0.999995	0.7078	0.2827	IIF
G10	0.0000	0.0000	0.0052	0.0009	0.9999	0.999998	0.4943	0.1611	IIF
G11	0.0000	0.0000	0.0117	0.0024	0.9998	0.999990	1.3365	0.4985	IIR
G12	0.0000	0.0000	0.0128	0.0018	0.9996	0.999991	0.4893	0.1810	IIRM
G13	0.0000	0.0000	0.0100	0.0014	0.9997	0.999994	0.4367	0.1378	IIR
G14	0.0000	0.0000	0.0098	0.0014	0.9997	0.999995	0.4811	0.1623	IIR
G15	0.0000	0.0000	0.0109	0.0019	0.9995	0.999984	0.9718	0.3886	IIRM
G16	0.0000	0.0000	0.0122	0.0018	0.9997	0.999993	0.6185	0.2191	IIR
G17	0.0000	0.0000	0.0166	0.0037	0.9991	0.999957	2.4014	0.9561	IIRM
G19	0.0000	0.0000	0.0104	0.0014	0.9997	0.999995	0.3356	0.0668	IIR
G20	0.0000	0.0000	0.0110	0.0017	0.9996	0.999989	0.7361	0.2965	IIR
G21	0.0000	0.0000	0.0147	0.0027	0.9991	0.999971	1.1309	0.3857	IIR
G22	0.0000	0.0000	0.0103	0.0013	0.9997	0.999995	0.3049	0.0594	IIR
G23	0.0000	0.0000	0.0104	0.0019	0.9996	0.999988	1.0675	0.3621	IIR
G24	0.0001	0.0000	0.0332	0.0084	0.9993	0.999956	5.2809	2.0991	IIF
G25	0.0000	0.0000	0.0060	0.0013	0.9999	0.999995	0.6938	0.2779	IIF
G26	-0.0001	0.0000	0.0051	0.0015	0.9999	0.999994	0.3571	0.3395	IIF
G27	0.0000	0.0000	0.0061	0.0013	0.9999	0.999994	0.7030	0.2792	IIF
G28	0.0000	0.0000	0.0208	0.0060	0.9997	0.999976	3.8039	1.5210	IIR
G29	0.0000	0.0000	0.0135	0.0028	0.9991	0.999960	1.5520	0.6165	IIRM
G30	0.0000	0.0000	0.0070	0.0016	0.9998	0.999989	0.9766	0.3905	IIF
G31	0.0000	0.0000	0.0122	0.0025	0.9996	0.999982	1.5132	0.6042	IIRM
G32	0.0000	0.0000	0.0063	0.0013	0.9999	0.999994	0.7064	0.2419	IIF

Table 4-16 CLK11 RF statistical assessment for GLONASS satellites

Satellite #	Mean(m)		Standard deviation(m)		R ² Score		Range(m)		Satellite Block
	Latency	RF	Latency	RF	Latency	RF	Latency	RF	
R01	0.0000	0.0002	0.0281	0.0077	0.9983	0.99987	1.1437	0.4505	M
R02	0.0000	0.0001	0.0328	0.0084	0.9996	0.99997	3.6820	1.4709	M
R03	0.0000	0.0001	0.0225	0.0080	0.9993	0.99995	1.7044	1.5692	M
R05	0.0000	-0.0001	0.0215	0.0057	0.9990	0.99993	2.5159	1.0036	M
R07	0.0000	-0.0002	0.0263	0.0071	0.9991	0.99994	1.6672	0.6660	M
R08	0.0001	-0.0001	0.0397	0.0111	0.9994	0.99996	5.9137	2.3543	M
R09	0.0000	0.0000	0.0210	0.0059	0.9995	0.99997	2.8091	1.1203	K
R11	-0.0001	-0.0001	0.0267	0.0083	0.9997	0.99997	3.5225	1.4066	M
R12	0.0001	0.0000	0.0202	0.0054	0.9995	0.99997	2.5288	1.0082	M
R13	0.0001	-0.0002	0.0379	0.0094	0.9995	0.99997	4.8305	1.9179	M
R14	0.0000	0.0002	0.0230	0.0063	0.9995	0.99996	1.4032	0.5572	M
R15	0.0000	0.0000	0.0162	0.0042	0.9998	0.99998	1.1296	0.4452	M
R16	0.0001	0.0000	0.0279	0.0076	0.9995	0.99997	2.8219	1.1251	M
R17	0.0000	0.0001	0.0243	0.0065	0.9987	0.99991	1.1255	0.4485	M
R18	0.0001	0.0001	0.0297	0.0082	0.9996	0.99997	2.8272	1.1209	M
R19	0.0001	-0.0001	0.0234	0.0059	0.9991	0.99994	1.1371	0.4181	M
R20	-0.0001	-0.0001	0.0275	0.0074	0.9987	0.99990	1.9539	0.7767	M
R21	0.0000	0.0000	0.0189	0.0049	0.9991	0.99994	2.2431	0.8931	M
R22	-0.0001	-0.0001	0.0323	0.0091	0.9996	0.99997	3.9373	1.5703	M
R23	0.0001	0.0002	0.0299	0.0083	0.9990	0.99993	1.1330	0.7347	M

The upper part of the Figure 4-11 shows the RF model with original values for satellite G01, with respect to the prediction values obtained with RF for the CLK11 correction file, while the lower part shows the difference in meter between original and prediction values. While Figure 4-12 is the histogram that shows the frequency and the distribution of the differences.

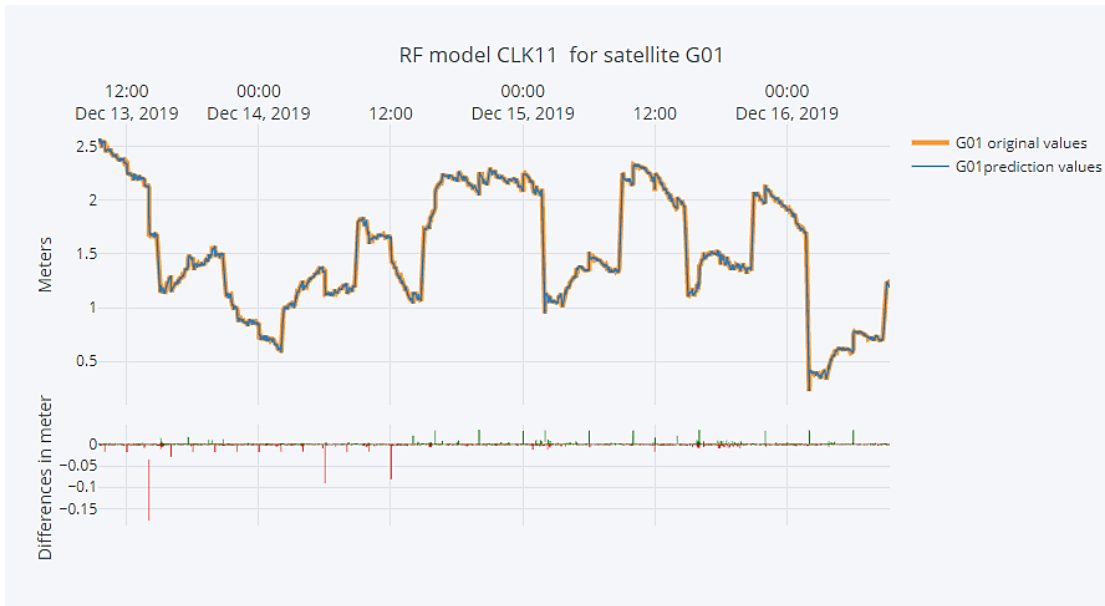


Figure 4-11 CLK11 RF model for satellite G01

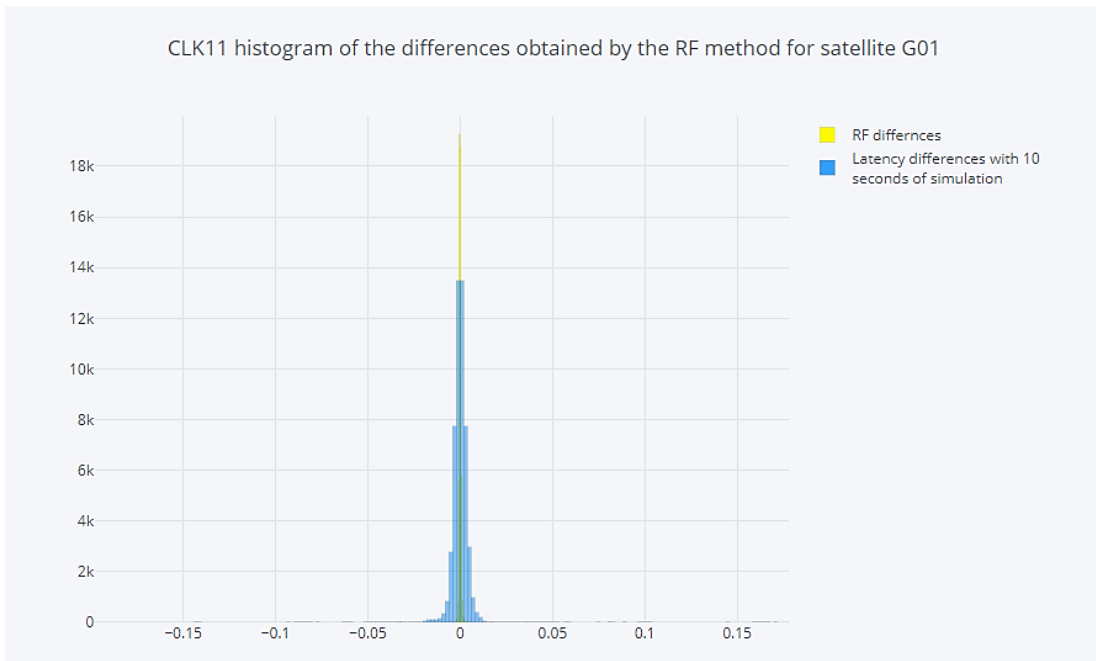


Figure 4-12 CLK11 histogram of the differences obtained by the RF method for satellite G01

Chapter 5 Conclusion and Future works

5.1 Conclusion

This study introduces two machine learning tools to overcome latency in correction products. The SVR and RF are used to solve the latency in the CLK11 and IGS03 correction files. The evaluation of the performance for the used machine learning tools was achieved by recreating the original correction files with simulated latency of 10 and 30 seconds for CLK11 and IGS03, respectively, which more or less the same latency experienced by the GNSS users.

Consequently, the differences are calculated between correction values produced by the analysis centers, which are free of latency with the correction values recreated with simulated latency, which simulates the GNSS user who is suffering from the latency. Simultaneously, the differences between prediction values produced by the machine learning tools are calculated with respect to the value produced by the analysis centers. Thus, the mean, standard deviation, maximum, minimum, and R2 score are used to evaluate the performance of SVR and RF. The following tables represent the overview of the statistical assessment phase. However, the SVR columns represent the Support vector regression solution, and RF columns represent the RandomForest solutions; each row represents the statistical values for each GNSS block.

Table 5-1 IGS03 SVR statistical assessment summary

Satellite Block	Mean(m)		Standard deviation(m)		R ² Score		Range(m)	
	Latency	SVR	Latency	SVR	Latency	SVR	Latency	SVR
IIF	0.0000	0.0000	0.0167	0.0233	0.9972	0.9971	1.2186	3.5276
IIR	0.0000	0.0000	0.0253	0.0247	0.987	0.9924	0.9972	2.3061
IIRM	0.0000	0.0000	0.0278	0.0247	0.988	0.9926	1.2164	2.4843
K	0.0001	-0.0002	0.0373	0.0514	0.9976	0.9955	2.8167	7.523
M	0.0000	-0.0001	0.0459	0.0553	0.9953	0.9944	2.3535	8.123

Table 5-2 is a repetition of Table 5-1 after removing the outliers.

Table 5-2 IGS03 SVR statistical assessment summary

Satellite Block	Mean(m)		Standard deviation(m)		R ² Score		Range(m)	
	Latency	SVR	Latency	SVR	Latency	SVR	Latency	SVR
IIF	0.0000	0.0000	0.0166	0.0112	0.9972	0.9986	1.2185	1.0051
IIR	0.0000	0.0000	0.0253	0.0175	0.9870	0.9937	0.9972	0.724
IIRM	0.0000	0.0000	0.0278	0.0196	0.9879	0.9939	1.2164	1.0295
K	0.0001	0.0001	0.0373	0.0258	0.9976	0.9989	2.8167	2.1808
M	0.0000	-0.0000	0.0458	0.0351	0.995284	0.9971	2.3534	2.7942

Table 5-3 CLK11 SVR statistical assessment summary

Satellite Block	Mean(m)		Standard deviation(m)		R ² Score		Range(m)	
	Latency	SVR	Latency	SVR	Latency	SVR	Latency	SVR
IIF	0.0000	0.0000	0.0096	0.0128	0.9998	0.9996	1.2324	1.2169
IIR	0.0000	0.0001	0.012	0.0181	0.9996	0.999	1.0145	0.3496
IIRM	0.0000	0.0000	0.0133	0.0201	0.9994	0.9986	1.204	0.7097
K	0.0000	0.0001	0.021	0.0266	0.9995	0.9993	2.8091	2.2349
M	0.0000	-0.0001	0.0268	0.0275	0.9993	0.9993	2.4853	2.2979

Table 5-4 IGS03 RF statistical assessment summary

Satellite Block	Mean(m)		Standard deviation(m)		R ² Score		Range(m)	
	Latency	RF	Latency	RF	Latency	RF	Latency	RF
IIF	0	0	0.0167	0.003	0.9972	0.9999	1.2186	0.2586
IIR	0	0	0.0253	0.0045	0.987	0.9996	0.9972	0.2332
IIRM	0	0	0.0278	0.0048	0.988	0.9996	1.2164	0.2463
K	0.0001	0	0.0373	0.0067	0.9976	0.9999	2.8167	0.5587
M	0	0	0.0459	0.0073	0.9953	0.9999	2.3535	0.4803

Table 5-5 CLK11 RF statistical assessment summary

Satellite Block	Mean(m)		Standard deviation(m)		R ² Score		Range(m)	
	Latency	RF	Latency	RF	Latency	RF	Latency	RF
IIF	0	0	0.0096	0.0022	0.9998	0.9999	1.2186	0.4958
IIR	0	0	0.0119	0.0021	0.9996	0.9999	0.9972	0.3703
IIRM	0	0	0.0132	0.0024	0.9994	0.9999	1.2164	0.4728
K	0.0001	0	0.0210	0.0059	0.9995	0.9999	2.8167	1.1202
M	0	0	0.0267	0.0073	0.9992	0.9999	2.3535	1.0493

From this study, we conclude that:

- For the RF method, the results were showing that the RF reduced the standard deviation as well as the range difference for both correction files. Besides, the mean of the differences calculated with respect to the prediction values is closer to zero. Furthermore, the R^2 score performed much better in comparison to the latency solution.
- For the SVR, the results were showing that the SVR reduced the standard deviation as well as the range difference for the IGS03 file. In addition, the SVR behaves similarly to the RF with respect to the R^2 score and the mean of the differences. However, for the CLK11, the SVR did not reduce the standard deviation, as well as the mean values, remain the same more or less, but the range differences are reduced significantly for the CLK11. This indicates that the SVR was able to reduce the dispersion or, in other words, the range even if it slightly increase the standard deviation.

5.2 Future works

It is recommended to reapply the proposed methodology in this research with different sliding windows intervals, as well as applying the GridSearchCV for SVR with different search parameters. In this research, the RF implements with default values, and it is suggested to reapply the RF method with GridSearchCV in order to tune the RandomForest Regressor.

We propose to apply different machine learning tools such as neural networks to solve the latency problem. The BNC software can run the PPP with post-process mode. Thus it is recommended to rerun the BNC in post-processing mode, with the prediction values obtained by the SVR or the RF, to examine the quality of the coordinates with the influence of the prediction models. We also propose to apply this research to solve latency in other IGS products such as CLK93, CLK51, IGS01, and IGS02... etc. Besides the statistical assessment done in this research, it is recommended to investigate the prediction values with Wilcoxon signed ranks test or another statistical test to check if there is a significant difference between latency and prediction values.

References

- Alcay, S., & Turgut, M. (2017). Performance Evaluation of Real-Time Precise Point Positioning Method. *IOP Conference Series: Earth and Environmental Science*, 95(3). <https://doi.org/10.1088/1755-1315/95/3/032023>
- Awad, M., & Khanna, R. (2015). Efficient learning machines: Theories, concepts, and applications for engineers and system designers. *Efficient Learning Machines: Theories, Concepts, and Applications for Engineers and System Designers*, (January), 1–248. <https://doi.org/10.1007/978-1-4302-5990-9>
- B.Hoffmann-Wellenhof, & H.Lichtenegg. (2001). *Global positioning system, theory and practice, 5th edition. Eos, Transactions American Geophysical Union* (Fifth edit, Vol. 82). <https://doi.org/10.1029/01eo00224>
- Barker, R., Lapucha, D., & Wood, T. (2002). The Impact of High Performance GPS on the Offshore Marine Survey, Navigation and Positioning Industry. *Offshore Technology Conference*. Houston, Texas: Offshore Technology Conference. <https://doi.org/10.4043/14195-MS>
- Beskyroun, S., Wegner, L. D., & Sparling, B. F. (2011). Integral resonant control scheme for cancelling human-induced vibrations in light-weight pedestrian structures. *Structural Control and Health Monitoring*, (May 2011), n/a-n/a. <https://doi.org/10.1002/stc>
- Bezcioglu, M., Yigit, C. O., & El-mowafy, A. (2019). Kinematic PPP-AR in Antarctic, (April).
- Blewitt, G. (2019). Basics of the GPS technique: observation equations.
- Blewitt, G., Hammond, W. C., Kreemer, C., Plag, H. P., Stein, S., & Okal, E. (2009). GPS for real-time earthquake source determination and tsunami warning systems. *Journal of Geodesy*, 83(3–4), 335–343. <https://doi.org/10.1007/s00190-008-0262-5>
- Breiman, L. (2001). ST4_Method_Random_Forest. *Machine Learning*, 45(1), 5–32. <https://doi.org/10.1017/CBO9781107415324.004>
- Buntine, W., & Niblett, T. (1992). A further comparison of splitting rules for decision-tree induction. *Machine Learning*, 8(1), 75–85. <https://doi.org/10.1007/bf00994006>
- Capilla, R. M., Berné, J. L., Martín, A., & Rodrigo, R. (2016). Simulation case study of deformations and landslides using real-time GNSS precise point positioning technique. *Geomatics, Natural Hazards and Risk*, 7(6), 1856–1873. <https://doi.org/10.1080/19475705.2015.1137243>
- Cernigliaro, A., Valloreia, S., Galleani, L., & Tavella, P. (2013). GNSS space clocks: Performance analysis. *2013 International Conference on Localization and GNSS, ICL-GNSS 2013*, 1–5. <https://doi.org/10.1109/ICL-GNSS.2013.6577251>

- Chen, J., Li, H., Wu, B., Zhang, Y., Wang, J., & Hu, C. (2013). Performance of Real-Time Precise Point Positioning. *Marine Geodesy*, 36(1), 98–108. <https://doi.org/10.1080/01490419.2012.699503>
- Cina, A., & Piras, M. (2015). Performance of low-cost GNSS receiver for landslides monitoring: test and results. *Geomatics, Natural Hazards and Risk*, 6(5–7), 497–514. <https://doi.org/10.1080/19475705.2014.889046>
- Clarkson, K. L., Hazan, E., & Woodruff, D. P. (2012). *Sublinear optimization for machine learning*. *Journal of the ACM* (Vol. 59). <https://doi.org/10.1145/2371656.2371658>
- Dodson, A. H. (1986). Refraction and propagation delays in space geodesy. *International Journal of Remote Sensing*, 7(4), 515–524. <https://doi.org/10.1080/01431168608954706>
- Dong, X., Yang, L., Zhu, Q., Guo, C., Zhao, Z., & Lin, L. (2018). A Method of Retrieving Tropospheric Refractivity Above Ocean Surface using GNSS. In *2018 12th International Symposium on Antennas, Propagation and EM Theory (ISAPE)* (pp. 1–4). <https://doi.org/10.1109/ISAPE.2018.8634353>
- El-Mowafy, A. (2019). Predicting orbit and clock corrections during their outage in real-time positioning using GPS, GLONASS and QZSS for natural hazard warning systems. *Journal of Applied Geodesy*, 13(2), 69–79. <https://doi.org/10.1515/jag-2018-0043>
- El-Mowafy, A., & Deo, M. (2017). Bridging Real-Time Precise Point Positioning in Natural Hazard Warning Systems during Outages of MADOCA Corrections. *Proceedings of the ION 2017 Pacific PNT Meeting*, (January 2019), 514–525. <https://doi.org/10.33012/2017.15075>
- El-Mowafy, A., Deo, M., & Kubo, N. (2017). Maintaining real-time precise point positioning during outages of orbit and clock corrections. *GPS Solutions*, 21(3), 937–947. <https://doi.org/10.1007/s10291-016-0583-4>
- El-Rabbany, A. (2002). *Introduction to GPS: the global positioning system*.
- Enge, P., & Misra, P. (2011). *Global Positioning System: Signals, Measurements, and Performance - Revised Second Edition (2011)* (Second Edi).
- Erdogan, B., & Karlitepe, F. (2016). EXPERIMENTS ON REAL-TIME PRECISE POINT POSITIONING (RT-PPP). <https://doi.org/10.13140/RG.2.2.31028.04486>
- European GNSS Service Centre. (2020). Constellation Information | European GNSS Service Centre. Retrieved December 10, 2019, from <https://www.gsc-europa.eu/system-service-status/constellation-information>
- Fugro. (2016). Group overview | Fugro. Retrieved December 23, 2019, from <https://www.fugro.com/about-fugro/group-overview>

- Ge, M., Chen, J., Douša, J., Gendt, G., & Wickert, J. (2012). A computationally efficient approach for estimating high-rate satellite clock corrections in realtime. *GPS Solutions*, *16*(1), 9–17. <https://doi.org/10.1007/s10291-011-0206-z>
- Geng, J. (2016). Rapid Re-convergence in Real-time Precise Point Positioning with Ambiguity Resolution, (January 2009).
- Georg Weber, Leoš Mervart , Andrea Stürze , Axel Rülke, D., & Stöcker. (2016). *BNC Help*.
- Hadas, T., & Bosy, J. (2014). IGS RTS precise orbits and clocks verification and quality degradation over time. *GPS Solutions*, *19*(1), 93–105. <https://doi.org/10.1007/s10291-014-0369-5>
- Hristopoulos, D. T., Mertikas, S. P., Arhontakis, I., & Brownjohn, J. M. W. (2007). Using GPS for monitoring tall-building response to wind loading: Filtering of abrupt changes and low-frequency noise, variography and spectral analysis of displacements. *GPS Solutions*, *11*(2), 85–95. <https://doi.org/10.1007/s10291-006-0035-7>
- Hsu, L. (2017). GNSS multipath detection using a machine learning approach. In *2017 IEEE 20th International Conference on Intelligent Transportation Systems (ITSC)* (pp. 1–6). <https://doi.org/10.1109/ITSC.2017.8317700>
- Huang, G. W., Zhang, Q., & Xu, G. C. (2014). Real-time clock offset prediction with an improved model. *GPS Solutions*, *18*(1), 95–104. <https://doi.org/10.1007/s10291-013-0313-0>
- Huang, G., & Zhang, Q. (2012). Real-time estimation of satellite clock offset using adaptively robust Kalman filter with classified adaptive factors. *GPS Solutions*, *16*(4), 531–539. <https://doi.org/10.1007/s10291-012-0254-z>
- I. Guyon, B. Boser, & V. Vapnik. (1993). Automatic Capacity Tuning of Very Large VC-Dimension Classifiers. *Advances in Neural Information Processing Systems*, *5*, 147–155. Retrieved from <http://www.clopinet.com/isabelle/Papers/autocapa.ps>
- IGS. (2020). IGS Station - BRST00FRA. Retrieved January 16, 2020, from http://www.igs.org/igsnetwork/network_by_site.php?site=brst00fra
- Information and Analysis Center. (2020). INFORMATION AND ANALYSIS CENTER FOR POSITIONING, NAVIGATION AND TIMING. Retrieved December 10, 2019, from <https://www.glonass-iac.ru/en/GPS/>
- International Earth Rotation and Reference System Service. (2013). The International Terrestrial Reference Frame (ITRF). Retrieved January 8, 2020, from <https://www.iers.org/IERS/EN/DataProducts/ITRF/itrf.html>
- Johnston, G., Riddell, A., & Hausler, G. (2017). The International GNSS Service. *Springer Handbook of Global Navigation Satellite Systems*, 967–982.

https://doi.org/10.1007/978-3-319-42928-1_33

Juan, J. M., Hernández-Pajares, M., Sanz, J., Ramos-Bosch, P., Aragón-Ángel, A., Orús, R., ... Tossaint, M. (2012). Enhanced Precise Point Positioning for GNSS users. *IEEE Transactions on Geoscience and Remote Sensing*, 50(10 PART2), 4213–4222. <https://doi.org/10.1109/TGRS.2012.2189888>

Kalooop, M. R., Elbeltagi, E., Hu, J. W., & Elrefai, A. (2017). Recent advances of structures monitoring and evaluation using GPS-Time series monitoring systems: A review. *ISPRS International Journal of Geo-Information*, 6(12). <https://doi.org/10.3390/ijgi6120382>

Kaplan & Hegrat. (2006). *Understanding GPS*. (Elliott D. Kaplan Christopher J. Hegarty, Ed.), *Better Corporate Reporting* (Second Edi). <https://doi.org/10.4324/9781351274845-10>

Khoo, V. H. S., Tor, Y. K., & Ong, G. (2010). Monitoring of High Rise Building using Real-Time Differential GPS Monitoring of High Rise Building using Real-Time Differential GPS. *FIG Congress 2010 Facing Challenges- Building the Capacity*, (April), 11–16. Retrieved from http://www.fig.net/pub/fig2010/papers/ts02d%5Cts02d_khoo_tor_et_al_3976.pdf

Kouba, J., & Héroux, P. (2001). Precise Point Positioning Using IGS Orbit and Clock Products. *GPS Solutions*, 5(2), 12–28. <https://doi.org/10.1007/PL00012883>

Kumar, S., Bhattacharyya, B., & Gupta, V. K. (2014). Present and Future Energy Scenario in India. *Journal of The Institution of Engineers (India): Series B*, 95(3), 247–254. <https://doi.org/10.1007/s40031-014-0099-7>

Labrecque, J., Rundle, J., & Bawden, G. (2018). Global Navigation Satellite System to Enhance Tsunami Early Warning Systems, (December).

Martín, A., Anquela, A. B., Dimas-Pagés, A., & Cos-Gayón, F. (2015). Validation of performance of real-time kinematic PPP. A possible tool for deformation monitoring. *Measurement: Journal of the International Measurement Confederation*, 69, 95–108. <https://doi.org/10.1016/j.measurement.2015.03.026>

Martín, A., Hadas, T., Dimas, A., & Anquela, A. B. (2013). INFLUENCE OF REAL-TIME PRODUCTS LATENCY ON KINEMATIC PPP RESULTS, (1), 1–4.

Math behind SVM(Support Vector Machine). (2019). Retrieved January 17, 2020, from <https://mc.ai/math-behind-svmsupport-vector-machine/>

Matplotlib. (2012). Matplotlib: Python plotting — Matplotlib 3.1.2 documentation. Retrieved January 15, 2020, from <https://matplotlib.org/>

Mongillo, M. (2011). Choosing Basis Functions and Shape Parameters for Radial

- Basis Function Methods. *SIAM Undergraduate Research Online*, 4, 190–209. <https://doi.org/10.1137/11s010840>
- National Geodetic Survey. (2019). Antenna Calibrations. Retrieved January 3, 2020, from <https://www.ngs.noaa.gov/ANTCAL/>
- Niell, A. E. (1996). Global mapping functions for the atmosphere delay at radio wavelengths. *Journal of Geophysical Research: Solid Earth*, 101(B2), 3227–3246. <https://doi.org/10.1029/95jb03048>
- Noël, S. (2012). Rise in upper-atmospheric carbon. *Nature Geoscience*, 5(12), 848–849. <https://doi.org/10.1038/ngeo1648>
- NovAtel. (2015). NovAtel CORRECT® with PPP | NovAtel. Retrieved December 23, 2019, from <https://www.novatel.com/products/novatel-correct-ppp/>
- NovAtel Inc, . (2015). *An Introduction to GNSS GPS, GLONASS, BeiDou, Galileo and other Global Navigation Satellite Systems NovAtel*. Retrieved from <https://www.novatel.com/assets/Documents/Books/Intro-to-GNSS.pdf%0Ahttps://www.novatel.com/an-introduction-to-gnss/>
- Nüst, D., Granell, C., Hofer, B., Konkol, M., Ostermann, F. O., Sileryte, R., & Cerutti, V. (2018). Reproducible research and GIScience: An evaluation using AGILE conference papers. *PeerJ*, 2018(7), 1–23. <https://doi.org/10.7717/peerj.5072>
- P. Daly, I. D. K. (1990). Characterization of NAVSTAR GPS and GLONASS On-Board Clocks.
- Parang, K., Wiebe, L., & Knaus, E. (2012). *AN Introduction to Statistical Learning. Current Medicinal Chemistry* (Vol. 7). <https://doi.org/10.2174/0929867003374372>
- Piras, M., & Roggero, M. (2009). Volume 13: Solid Earth (SE), 13(October 2016). <https://doi.org/10.1142/9789812836182>
- Plotly. (2018). Plotly | Make charts and dashboards online. Retrieved January 15, 2020, from <https://chart-studio.plot.ly/feed/#/>
- Pollard, R. J. (2009). Essentials of Satellite Navigation, 30. <https://doi.org/10.1177/014662168400800314>
- python organization. (2016). Welcome to Python.org. Retrieved January 15, 2020, from <https://www.python.org/>
- Quinlan, J. R. (1986). Induction of decision trees. *Machine Learning*, 1(1), 81–106. <https://doi.org/10.1007/bf00116251>
- Rizos, C., & Cranenbroeck, J. Van. (2010). Advances in GNSS-RTK for Structural Deformation Monitoring in Regions of High Ionospheric Activity Advances in

- GNSS-RTK for Structural Deformation Monitoring in Regions of High Ionospheric Activity-Presentation. *Information Systems*, (April), 11–16.
- RTCM Special Committee. (2016). *RTCM Standard 10403.3 differential GNSS (Global Navigation Satellite Systems) Services-Version 3*. Arlington, TX, USA.
- Sánchez-Naranjo, S., González, F. A., Ramos-Pollán, R., & Solé, M. (2016). Data driven Vertical Total Electron Content workflow for GNSS positioning for single frequency receivers. In *2016 International Conference on Localization and GNSS (ICL-GNSS)* (pp. 1–6). <https://doi.org/10.1109/ICL-GNSS.2016.7533862>
- Şanlıoğlu, İ., Zeybek, M., & Özer Yiğit, C. (2016). Landslide Monitoring with GNSS-PPP on Steep-Slope and Forestry Area: Taşkent Landslide. *ICENS International Conference on Engineering and Natural Science*, (September), 1–7.
- Sanz Subirana, J. M. J. Z. and M. H.-P. (2013). *Gnss Data Processing* (Vol. I).
- Schmid, R., Steigenberger, P., & Gendt, G. (2007). Generation of a Consistent Absolute Phase Center Correction Model for GPS Receiver and Satellite Antennas. <https://doi.org/10.1007/s00190-007-0148-y>.Ralf
- SciKit-Learn. (2016). scikit-learn: machine learning in Python — scikit-learn 0.22.1 documentation. Retrieved January 15, 2020, from <https://scikit-learn.org/stable/index.html>
- Scornet, E. (2017). Tuning parameters in random forests. *ESAIM: Proceedings and Surveys*, 60(2001), 144–162. <https://doi.org/10.1051/proc/201760144>
- Seaborn. (2012). seaborn: statistical data visualization — seaborn 0.9.0 documentation. Retrieved January 16, 2020, from <https://seaborn.pydata.org/>
- Senior, K. L., Ray, J. R., & Beard, R. L. (2008). Characterization of periodic variations in the GPS satellite clocks. *GPS Solutions*, 12(3), 211–225. <https://doi.org/10.1007/s10291-008-0089-9>
- Shamshiri, R., Motagh, M., Nahavandchi, H., Haghshenas Haghghi, M., & Hoseini, M. (2020). Improving tropospheric corrections on large-scale Sentinel-1 interferograms using a machine learning approach for integration with GNSS-derived zenith total delay (ZTD). *Remote Sensing of Environment*, 239, 111608. <https://doi.org/https://doi.org/10.1016/j.rse.2019.111608>
- Shi, J., Xu, C., & Guo, J. (2013). A Performance Analysis of Real-Time Precise Point Positioning for Deformation Monitoring, (November 2015).
- SMOLA, A. J. and B. S. (2004). A tutorial on support vector regression - [art%3A10.1023%2FB%3ASTCO.0000035301.49549.88.pdf](https://arxiv.org/abs/1010.2323). *Statistics and Computing*, 14, 199–222. <https://doi.org/10.1023/B:STCO.0000035301.49549.88>

- Sundaramoorthy, P., Gill, E., Verhoeven, C., & Bouwmeester, J. (2010). Two CubeSats with Micro-Propulsion in the QB50 Satellite Network. *24th Annual AIAA/USU Conference on Small Satellites*, (January 2010), 1–11. Retrieved from <http://digitalcommons.usu.edu/smallsat/2010/all2010/17/>
- Tang, X., Roberts, G. W., Li, X., & Hancock, C. M. (2017). Real-time kinematic PPP GPS for structure monitoring applied on the Severn Suspension Bridge, UK. *Advances in Space Research*, *60*(5), 925–937. <https://doi.org/10.1016/j.asr.2017.05.010>
- The International GNSS Service. (2013). IGS RTS Products. Retrieved December 16, 2019, from <http://www.igs.org/rts/products>
- The Multi-GNSS Experiment and Pilot Project (MGEX). (2016). IGS MGEX. Retrieved December 23, 2019, from <http://mgex.igs.org/index.php>
- Trimble. (2012). High Precision RTX Technology | Trimble GNSS Positioning. Retrieved December 23, 2019, from <https://positioningservices.trimble.com/services/rtx/>
- U.S.Department of Homeland security. (2020). Navigation Center. Retrieved January 23, 2020, from <https://www.navcen.uscg.gov/?Do=constellationStatus>
- Wächter, J., Babeyko, A., Fleischer, J., Häner, R., Hammitzsch, M., Kloth, A., & Lendholt, M. (2012). Development of tsunami early warning systems and future challenges. *Natural Hazards and Earth System Science*, *12*(6), 1923–1935. <https://doi.org/10.5194/nhess-12-1923-2012>
- Wang, L., Li, Z., Ge, M., Neitzel, F., Wang, Z., & Yuan, H. (2018). *Validation and Assessment of Multi-GNSS Real-Time Precise Point Positioning in Simulated Kinematic Mode Using IGS Real-Time Service*. *Remote Sensing* (Vol. 10). <https://doi.org/10.3390/rs10020337>
- Wang, Z., Li, Z., Wang, L., Wang, X., & Yuan, H. (2018). Assessment of Multiple GNSS Real-Time SSR Products from Different Analysis Centers. *ISPRS International Journal of Geo-Information*, *7*(3), 85. <https://doi.org/10.3390/ijgi7030085>
- Weber, G., Dettmering, D., & Gebhard, H. (2005). Networked Transport of RTCM via Internet Protocol (NTRIP) BT - A Window on the Future of Geodesy. In F. Sansò (Ed.) (pp. 60–64). Berlin, Heidelberg: Springer Berlin Heidelberg.
- Wells, D. (1999). *GUIDE TO GPS POSITIONING*.
- Wolf, P. R., & Wiley, J. (2006). *ADJUSTMENT* (Fourth edi).
- Wu, J., Wu, S., Hajj, G., Bertiger, W., & Lichten, S. (1992). Effects of Antenna Orientation on GPS Carrier Phase. *Manuscr. Geod.*, *18*.
- Yang, H., Xu, C., & Gao, Y. (2019). Analysis of GPS satellite clock prediction

- performance with different update intervals and application to real-time PPP. *Survey Review*, 51(364), 43–52.
<https://doi.org/10.1080/00396265.2017.1359473>
- Yao, Y., He, Y., Yi, W., Song, W., Cao, C., & Chen, M. (2017). Method for evaluating real-time GNSS satellite clock offset products. *GPS Solutions*, 21(4), 1417–1425. <https://doi.org/10.1007/s10291-017-0619-4>
- Yao, Y., Peng, W., Xu, C., & Cheng, S. (2017). Enhancing real-time precise point positioning with zenith troposphere delay products and the determination of corresponding tropospheric stochastic models. *Geophysical Journal International*, 208(2), 1217–1230. <https://doi.org/10.1093/gji/ggw451>
- Yuan, Y., Pan, L., Liu, J., Zhang, X., Guo, F., & Li, X. (2018). GPS inter-frequency clock bias modeling and prediction for real-time precise point positioning. *GPS Solutions*, 22(3), 0. <https://doi.org/10.1007/s10291-018-0741-y>
- Zhiping Liu, Q. Z. (2016). Dynamic GPS Precise Point Positioning for Deformation Monitoring Using Prior Information, (January 2015).
<https://doi.org/10.1007/978-3-662-46632-2>
- Zumberge, J. F., Heflin, M., Jefferson, D. C., Watkins, M., & Webb, F. (1997). Precise Point Positioning for the Efficient And Robust Analysis of GPS Data from Large Networks. *Journal of Geophysical Research*, 102.
<https://doi.org/10.1029/96JB03860>